Journal of Chemistry

Polymers and Upconversion Nanoparticles for Disease Diagnosis and Treatment

Lead Guest Editor: Ranjit De
Guest Editors: Bijan Das and Manoj K. Mahata

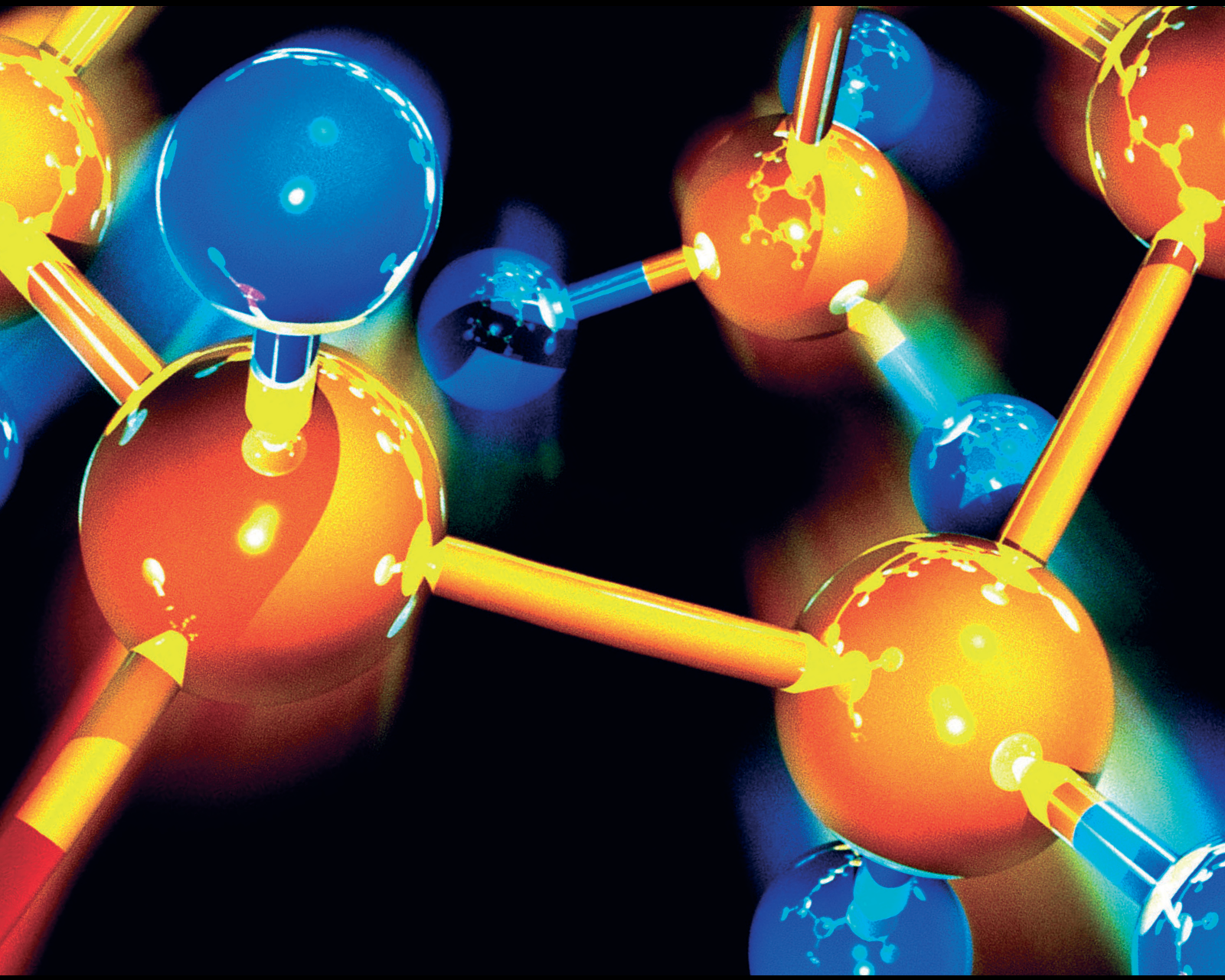

Polymers and Upconversion Nanoparticles for Disease Diagnosis and Treatment

Journal of Chemistry

Polymers and Upconversion Nanoparticles for Disease Diagnosis and Treatment

Lead Guest Editor: Ranjit De
Guest Editors: Bijan Das and Manoj K. Mahata

Chief Editor

Kaustubha Mohanty, India

Associate Editors

Mohammad Al-Ghouti, Qatar
Tingyue Gu, USA
Teodorico C. Ramalho, Brazil
Artur M. S. Silva, Portugal

Academic Editors

Jinwei Duan , China
Luqman C. Abdullah, Malaysia
Dr Abhilash, India
Amitava Adhikary, USA
Amitava Adhikary, USA
Mozhgan Afshari, Iran
Daryoush Afzali, Iran
Mahmood Ahmed, Pakistan
Islam Al-Akraa, Egypt
Juan D. Alché, Spain
Gomaa A. M. Ali, Egypt
Mohd Sajid Ali, Saudi Arabia
Shafaqat Ali, Pakistan
Patricia E. Allegretti, Argentina
Marco Anni, Italy
Alessandro Arcovito, Italy
Hassan Arida, Saudi Arabia
Umair Ashraf, Pakistan
Narcis Avarvari, France
Davut Avci, Turkey
Chandra Azad, USA
Mohamed Azaroual, France
Rasha Azzam, Egypt
Hassan Azzazy, Egypt
Renal Backov, France
Suresh Kannan Balasingam, Republic of Korea
Sukanta Bar, USA
Florent Barbault, France
Maurizio Barbieri, Italy
James Barker, United Kingdom
Salvatore Barreca, Italy
Jorge Barros-Velázquez, Spain
THANGAGIRI Baskaran, India
Haci Baykara, Ecuador
Michele Benedetti, Italy
Laurent Billon, France
Marek Biziuk, Poland
Jean-Luc Blin, France
Tomislav Bolanca, Croatia
Ankur Bordoloi, India
Cato Brede, Norway
Leonid Breydo, USA
Wybren J. Buma, The Netherlands
J. O. Caceres, Spain
Patrizia Calaminici, Mexico
Claudio Cameselle, Spain
Joaquin Campos, Spain
Dapeng Cao, China
Domenica Capasso, Italy
Stefano Caporali, Italy
Zenilda Cardeal, Brazil
Angela Cardinali, Italy
Stefano Carli, Italy
Maria F. Carvalho, Portugal
Susana Casal, Portugal
David E. Chavez, USA
Riccardo Chelli, Italy
Zhongfang Chen, Puerto Rico
Vladislav Chrastny, Czech Republic
Roberto Comparelli, Italy
Filomena Conforti, Italy
Luca Conti, Italy
Christophe Coquelet, France
Filomena Corbo, Italy
Jose Corchado, Spain
Maria N. D.S. Cordeiro, Portugal
Claudia Crestini, Italy
Gerald Culioli, France
Nguyen Duc Cuong, Vietnam
Stefano D'Errico, Italy
Matthias D'hooghe, Belgium
Samuel B. Dampare, Ghana
Umashankar Das, Canada
Victor David, Romania
Annalisa De Girolamo, Italy
Antonio De Lucas-Consuegra, Spain
Marcone A. L. De Oliveira, Brazil
Paula G. De Pinho, Portugal
Damião De Sousa, Brazil
Francisco Javier Deive, Spain
Tianlong Deng, China

Contents

Hindawi
Journal of Chemistry
Volume 2022, Article ID 7903310, 19 pages
https://doi.org/10.1155/2022/7903310

Research Article

Development and Evaluation of a Novel Polymer Drug Delivery System Using Cromolyn-Polyamides-Disulfide using Response Surface Design

Nadeen Mohammad Alkurdi,[1] Samer Hasan Hussein-Al-Ali,[1,2] Awad Albalwi,[3] Mike Kh. Haddad,[4] Yousef Aldalahmed,[1] and Dalia Khalil Ali[1,5]

[1]*Department of Basic Pharmaceutical Sciences, Faculty of Pharmacy, Isra University, Amman 11622, Jordan*
[2]*Department of Chemistry, Faculty of Science, Isra University, Amman 11622, Jordan*
[3]*Department of Chemistry, College of Science, King Saud University, Riyadh, Saudi Arabia*
[4]*Department of Renewable Energy Engineering, Faculty of Engineering, Isra University, P.O. Box 22, Amman 11622, Jordan*
[5]*Department of Physiotherapy, Faculty of Allied Medical Sciences, Isra University, Amman 11622, Jordan*

Correspondence should be addressed to Samer Hasan Hussein-Al-Ali; sameralali72@yahoo.com

Received 23 February 2022; Accepted 30 May 2022; Published 28 June 2022

Academic Editor: Ranjit De

The aim of this study was to employ nanoparticles as drug carriers. The research involved the design of cromolyn polyamide-disulfide nanocomposites to overcome the problem of frequent cromolyn doses and improve their properties. The cromolyn polyamide-disulfide samples were prepared using several amounts of cromolyn and sodium polyamide-disulfide polymer at different pH values. Analysis of variance (ANOVA) was performed to obtain the significant independent variables affecting the dependent response by using a P value lower than 0.05. The nanocomposites produced were characterized using Fourier transform infrared (FTIR) spectroscopy and in vitro release. An FTIR test was used to evaluate the functional groups of cromolyn in nanocomposites, which indicated that the drug was encapsulated inside the polymer. All data indicated the presence of cromolyn in the nanocomposites. The release profile of nanocomposites was found to be sustained. Therefore, the outcome of this research project could be a starting point for further work to optimize and assess polyamide-disulfide polymers for delivering another drug.

1. Introduction

Nanoparticles are a broad category of materials that include particulate substances with dimensions less than 100 nm. Nanoparticles are categorized into different groups based on their shapes, properties, and size and offer various advantages [1, 2], including sustained release in the gastrointestinal tract, GIT, better penetration, and excellent uptake by cells [3, 4]. Furthermore, these nanoparticles are biodegradable and nontoxic to cells. All these benefits enable them to be ideal candidates with improved effectiveness. There are several advantages of using nanoparticles in drug delivery, including improved stability in vivo, as well as long-term capacity for release and penetration through small capillaries and body compartments [3].

Nanoparticles may also improve drug bioavailability and enhance biodistribution properties and pharmacokinetics. The following are the primary criteria for nanoparticle delivery: high loading capacity, slow dissociation in vivo, and optimized targeting to the desired tissue with reduced absorption by other tissues. The production of formulations that have these characteristics, while being cost-effective and simple to design, is important for the development of an effective delivery system [5].

Polyamides and disulfide polymers were synthesized by interfacial polycondensation of diamines and cystine amino

acids with dicarbonyl dichlorides derived from renewable dicarboxylic acids [6].

Cromolyn was initially used to treat allergic asthma and soon has been shown to be successful in treating intestinal allergies, mastocytes, and allergic skin conditions. The mast cell stabilizer is widely used for its therapeutic function in the treatment of allergic diseases [7]. Cromolyn sodium is synthesized by linking two monochrome nuclei with a shared alkyl residue. It is unique in its mechanism of action and wide range of clinical applications, although cromolyn sodium has been approved for the treatment of asthma since 1973. It is a white, hydrated powder that is lipophobic and highly polar, and its highly ionized acid salt has a PKa of 2 [8]. Cromolyn can be administered via inhalation or through intranasal, oral, or ophthalmic routes [9]. Under the biopharmaceutical classification scheme, cromolyn is classified as a Class III compound (BCS). Cromolyn's high solubility and poor permeability make it difficult to absorb from the gastrointestinal tract. Two carboxyl groups make cromolyn very hydrophilic, hampering its absorption across the gastrointestinal tract (GIT) and resulting in poor bioavailability in the treatment of health issues [10].

We expect the drug to reach its location at a certain concentration and be sustained for a long time for effective treatment; however, the drug's effect can be limited by several factors, including drug destruction. As a result, studies are being conducted on how to enhance the drug reaction and analyze its association with other cells as well as its inability to penetrate tissues because of its chemical character. Some researchers have attempted to improve the drug response by adding polymers with various physicochemical properties [11, 12].

Our study aims to devise a simple method to obtain a safe, stable mucoadhesive nanoparticulate formulation that can retain cromolyn inside the nasal mucosa. The nanocomposites were characterized in terms of particle size, zeta potential, and %LE. Furthermore, in vitro release studies were performed to study the nanoparticles' ability to deliver the drug in the nasal cavity.

2. Materials and Methods

2.1. Materials. The following chemicals were obtained from commercial sources and used: cromolyn from Sigma, polysulfide polyamine polymer from Dr. Dalia, sodium hydroxide from Chem Co (England), phosphate-buffered saline solution, ferric chloride of 98% purity, and deionized water.

2.2. Preparation of Blank-Polymer Nanoparticles and Cromolyn-Polymer Nanocomposites. The modified method, called the inotropic gelation method, was used for the preparation of nanoparticles and nanocomposites [13, 14]. A solution of cromolyn, $FeCl_3$, was prepared in distilled water, and a polymer solution was prepared in 0.1 Molar of NaOH. The solution of cromolyn was mixed with the polymer solution. After that, the solution of $FeCl_3$ was added dropwise to the mixture of the drug and polymer under stirring, and the pH was adjusted to 4.4 and 2.2. The nanocomposites were stirred overnight to allow the formation of nanocomposites with uniform size. The nanocomposites were collected using centrifugation (11,000 rpm). The final product was washed three times using distilled water and dried to obtain the final dry powder.

2.3. Methodology

2.3.1. Modeling of Different Responses. In this study, we studied the effect of different independent variables (drug, $FeCl_3$, polymer concentrations, and pH value) on three responses. The %LE is the first response that was used as a parameter and is defined as the total amount of entrapped drug divided by the total weight of nanoparticles. Particle size and zeta potential were the second and third responses used in this study.

2.3.2. Full Factorial Design (FFD). According to the levels in Table 1 and the full factorial design in Table 2, 54 samples were prepared according to Minitab 18 software [15, 16].

2.3.3. Multiple Regression Method. Regression analysis was used to show a mathematical relationship between the responses (%LE, particle size, and zeta potential) and independent variables (cromolyn, polymer, $FeCl_3$, and pH) [17].

2.4. Determination of the %LE of Cromolyn. %LE of cromolyn in the prepared nanocomposites was measured using an ultracentrifugation system at 11000 rpm, and the absorbance for free drug in the supernatant was measured at λ_{max} of 326 nm using the following equation [18]:

$$\%\text{loading} = \frac{\text{total mass of cromolyn} - \text{total mass of free cromolyn}}{\text{mass of nanocomposites}} \times 100. \quad (1)$$

2.5. Determination of Particle Size and Zeta Potential. At 25°C, each sample was analyzed in triplicate. The samples were dispersed in distilled water for 15 minutes, and they were sonicated. The cuvette was filled and covered. The Malvern logo should be directed to the instrument front and the absence of bubbles in the cuvette should be checked. The software automatically defined the run numbers in each measurement.

Table 1: Levels of drug, $FeCl_3$, polymer, and pH factors.

Factor	Unit	Low level	Middle level	High level
Drug	gm	0.05	0.10	0.20
$FeCl_3$	gm	0.3	0.6	1.2
polymer	gm	0.05	0.10	0.20
pH	None	2.2	—	4.4

2.6. In Vitro Release Study of Cromolyn from Nanocomposites. The in vitro release of cromolyn from the nanocomposites was determined in PBS at pH 7.4 using a Perkin Elmer UV-vis spectrophotometer with λ_{max} of 326 nm. Suitable amount of nanocomposite was added to release media. The percentage release of cromolyn in PBS was obtained using the following equation [19]:

$$\%\text{release} = \frac{\text{mass of cromolyn at time t}}{\text{mass of cromolyn it nanocomposite}} \times 100. \quad (2)$$

2.7. Instrumentation. UV-vis spectra were measured to determine the release of cromolyn using a Shimadzu UV-1601 spectrophotometer. Fourier transform infrared (FTIR) spectroscopy spectra of the materials were recorded over the range of 400–4000 cm^{-1} on a Perkin Elmer spectrometer (model Smart UAIR-two). The zeta potential was measured at 25°C by dynamic light scattering (DLS) using a Malvern Zetasizer Nano ZS (Malvern Instruments, Malvern, UK). X-ray diffraction (XRD) technique was used in the range of 5–70° by XRD D5005 diffractometer with CuKα radiation (Siemens, Munich, Germany). Scanning electron microscopy (FE-SEM) was done using Zeiss LEO 1550 (Jena, Germany).

3. Results and Discussion

3.1. Multiple Linear Regression Analysis Using Full Quadratic. The result values of the three models are shown in Table 3. The *R*-squared, *R*-sq (adj), and *R*-sq (pred) values for %LE are 94.95%, 93.32%, and 90.48%, respectively. The difference between R^2 and adjusted R^2 was 2.84%, which showed a good result for the data.

Additionally, from Table 3, the *R*-squared, *R*-sq (adj), and *R*-sq (pred) values for zeta potential are 93.69%, 91.43%, and 87.10%. respectively. The difference between R^2 and adjusted R^2 was 4.33%, which showed a good result for the data.

After taking the source (liner and 2-way interaction) during data analysis, the software was used to build the equation for %LE and zeta potential models. Table 4 shows the equations for the %LE and zeta potential models.

3.2. ANOVA for %LE, Size, and Zeta Potential

3.2.1. ANOVA for %LE. Table 5 shows the ANOVA data analysis for %LE models. From the table, the linear interaction contains drug, $FeCl_3$, polymer, and PH, while the 2-way interaction contains six different ways (drug*$FeCl_3$, drug*polymer, drug*PH, $FeCl_3$*polymer, $FeCl_3$*PH, and polymer*PH). With further analysis of the data, we found that only PH as linear (drug*PH, $FeCl_3$*PH, and polymer*PH) had a *P* value greater than 0.05 and nonsignificant properties, while the other sources had significant properties.

Table 2: Matrix for full factorial design.

Run order	Drug (gm)	$FeCl_3$ (gm)	Polymer (gm)	PH
1	0.05	0.6	0.05	2.2
2	0.05	0.6	0.20	4.4
3	0.05	0.3	0.10	4.4
4	0.20	0.3	0.10	2.2
5	0.05	0.3	0.05	4.4
6	0.10	0.6	0.10	2.2
7	0.20	1.2	0.20	2.2
8	0.05	1.2	0.20	2.2
9	0.20	0.3	0.20	4.4
10	0.10	0.3	0.20	4.4
11	0.05	0.3	0.10	2.2
12	0.20	1.2	0.05	2.2
13	0.20	0.6	0.10	2.2
14	0.10	0.3	0.10	4.4
15	0.10	1.2	0.20	4.4
16	0.10	0.6	0.20	4.4
17	0.20	0.6	0.20	2.2
18	0.20	1.2	0.10	4.4
19	0.10	0.6	0.20	2.2
20	0.05	0.3	0.05	2.2
21	0.10	1.2	0.10	2.2
22	0.05	0.6	0.05	4.4
23	0.05	0.6	0.10	2.2
24	0.05	0.6	0.10	4.4
25	0.05	1.2	0.20	4.4
26	0.20	0.3	0.20	2.2
27	0.20	1.2	0.10	2.2
28	0.20	1.2	0.05	4.4
29	0.10	1.2	0.05	2.2
30	0.20	0.6	0.05	2.2
31	0.05	0.3	0.20	2.2
32	0.05	1.2	0.10	2.2
33	0.20	0.6	0.20	4.4
34	0.10	0.3	0.05	4.4
35	0.10	1.2	0.05	4.4
36	0.10	0.3	0.05	2.2
37	0.20	0.6	0.10	4.4
38	0.20	0.3	0.10	4.4
39	0.20	1.2	0.20	4.4
40	0.10	0.3	0.10	2.2
41	0.20	0.3	0.05	4.4
42	0.10	1.2	0.20	2.2
43	0.10	0.6	0.02	4.4
44	0.05	0.3	0.20	4.4
45	0.10	1.2	0.10	4.4
46	0.05	0.6	0.20	2.2
47	0.10	0.6	0.05	2.2
48	0.10	0.3	0.20	2.2
49	0.05	1.2	0.05	4.4
50	0.20	0.3	0.05	2.2
51	0.05	1.2	0.10	4.4
52	0.10	0.6	0.10	4.4
53	0.20	0.6	0.05	4.4
54	0.05	1.2	0.05	2.2

Table 3: Regression model for dependent variables.

	R-sq (pred)	*R*-sq (adj)	*R*-sq
90.48%	93.32%	94.95%	%LE
87.10%	91.43%	93.69%	Zeta potential

Table 4: The %LE and zeta potential equations.

%LE	=	0.58 + 327.7 drug + 3.66 $FeCl_3$ + 6.0 polymer + 0.17 pH −202.6 drug*$FeCl_3$ −570 drug*polymer + 14.20 drug*pH + 92.8 $FeCl_3$*polymer −1.99 $FeCl_3$*pH −11.41 polymer*pH
Zeta potential	=	67.8 + 144.1 drug −56.5 $FeCl_3$ + 127.0 polymer −22.88 pH + 42.0 drug*$FeCl_3$ −233 drug*polymer −48.1 drug*pH −13.4 $FeCl_3$*polymer + 25.78 FeCl3*pH −30.6 polymer*pH

Table 5: ANOVA data of LE.

Source	DF	Adj SS	Adj MS	*F* value	*T* value	VIF	*P* value
Model	10	6173.26	617.33	58.25	—	—	0.001
Linear	4	3771.58	942.89	88.97	—	—	0.001
Drug	1	2819.09	2819.09	266.00	16.31	1.20	0.001
$FeCl_3$	1	1162.33	1162.33	109.67	−10.47	1.34	0.001
Polymer	1	125.90	125.90	11.88	−3.45	1.31	0.002
pH	1	39.15	39.15	3.69	−1.92	1.22	0.064
2-Way interaction	6	1200.79	200.13	18.88	—	—	0.001
Drug*$FeCl_3$	1	755.44	755.44	71.28	−8.44	1.16	0.001
Drug*polymer	1	131.92	131.92	12.45	−3.53	1.43	0.001
Drug*pH	1	33.43	33.43	3.15	1.78	1.18	0.086
$FeCl_3$*polymer	1	139.76	139.76	13.19	3.63	1.22	0.001
$FeCl_3$*pH	1	24.20	24.20	2.28	−1.51	1.11	0.141
Polymer*pH	1	21.16	21.16	2.00	−1.41	1.11	0.168
Error	31	328.54	10.60	—	—	—	—
Total	41	6501.81	—	—	—	—	—

3.2.2. ANOVA for Zeta Potential. Table 6 shows the ANOVA data analysis for the zeta potential models. From the table, the linear interaction contains drug, $FeCl_3$, polymer, and PH, while the 2-way interaction contains six different ways (drug*$FeCl_3$, drug*polymer, drug*PH, $FeCl_3$*polymer, $FeCl_3$*PH, and polymer*PH). With further analysis of the data, we found that only $FeCl_3$ and PH as linear (drug*PH and $FeCl_3$*PH) had *P* values less than 0.05 and significant properties.

3.2.3. ANOVA for Particle Size. Table 7 shows the ANOVA data analysis for particle size models. From the table, the linear model contains drug, $FeCl_3$, polymer, and PH, while the 2-way interaction contains six different ways (drug*$FeCl_3$, drug*polymer, drug*PH, $FeCl_3$*polymer, $FeCl_3$*PH, and polymer*PH). With further analysis of the data, we found that the *P* value for the particle size model was nonsignificant (0.339 > 0.05), so the particle size model was removed from the work.

3.3. Evaluation of the Models

3.3.1. Pareto Chart of Responses Standardized Effect and Half Normal Plot of the Standardized Effects. A Pareto chart in Figure 1 is a graphical overview of the process factors and/or interactions of influence, in ranking order from the most influencing to the least influencing. A threshold line (*P* value 0.05) indicates the minimum magnitude of statistically significant effects. The insignificance of factors can also be reasserted from the half normal plot (Figures 2(a)and 2(b)), where the points that do not fall near the fitted line and the variables that have a small effect on the output response are usually centered around zero. The effect of A (cromolyn) has the highest standardized effect on %LE, followed by B, AB, BC, AC, and C. All the significances of the factors are shown in the half normal plot (Figure 1(a)).

Figure 1(b) shows that PH, $FeCl_3$, $FeCl_3$ * PH, and drug * PH passed the reference line at 2.05, which means that these factors greatly affect the zeta potential at the 0.05 level. Additionally, this plot made it clear that zeta potential was not highly dependent on polymer * PH, drug * $FeCl_3$, drug * polymer, polymer, drug, and $FeCl_3$ * polymer. The effect of D (PH) has the highest standardized effect on the zeta potential, followed by B, B, and AD. All the significances of the factors are shown in the half normal plot (Figure 1(b)).

From the results shown in Figure 1(c) and for the Pareto charts of particle size, it can be seen that the particle size was not significant for all factors.

3.3.2. Residual Plots for %LE and Zeta Potential. The normality of the data can be checked by the normal probability plot of the residual, high value of R^2, and approximate straight line of the normal probability plot, as presented in

Table 6: ANOVA results for zeta potential.

Source	DF	Adj SS	Adj MS	*F* value	*T* value	VIF	*P* value
Model	10	20062.1	2006.21	41.56	—	—	0.001
Linear	4	14610.4	3652.61	75.66	—	—	0.001
Drug	1	17.4	17.39	0.36	−0.60	1.31	0.553
$FeCl_3$	1	4322.6	4322.60	89.54	9.46	1.31	0.001
Polymer	1	19.3	19.26	0.40	−0.63	1.40	0.533
pH	1	6514.6	6514.65	134.95	−11.62	1.23	0.001
2-Way interaction	6	4517.6	752.94	15.60			0.001
Drug*$FeCl_3$	1	29.8	29.81	0.62	0.79	1.33	0.439
Drug*polymer	1	26.9	26.88	0.56	−0.75	1.27	0.462
Drug*pH	1	333.7	333.74	6.91	−2.63	1.22	0.014
$FeCl_3$*polymer	1	3.3	3.30	0.07	−0.26	1.19	0.796
$FeCl_3$*pH	1	3209.4	3209.43	66.48	8.15	1.38	0.001
Polymer*pH	1	123.5	123.54	2.56	−1.60	1.42	0.121
Error	28	1351.7	48.28	—	—	—	—
Total	38	21413.8	—	—	—	—	—

Table 7: ANOVA data of particle size.

Source	DF	Adj SS	Adj MS	*T* value	VIF	*P* value
Model	10	66952	6695.2	—	—	0.339
Linear	4	33543	8385.9	—	—	0.231
Drug	1	1041	1040.8	−0.43	1.14	0.672
$FeCl_3$	1	16719	16718.9	1.71	1.08	0.095
Polymer	1	1768	1768.1	0.56	1.17	0.581
pH	1	11510	11509.9	−1.42	1.11	0.164
2-Way interaction	6	26922	4487.0			0.585
Drug*$FeCl_3$	1	3082	3082.2	0.74	1.06	0.467
Drug*polymer	1	49	48.8	0.09	1.18	0.927
Drug*pH	1	1391	1391.4	−0.49	1.09	0.624
$FeCl_3$*polymer	1	16810	16809.9	−1.72	1.09	0.095
$FeCl_3$*pH	1	208	208.3	−0.19	1.04	0.849
Polymer*pH	1	3677	3677.4	−0.80	1.11	0.427
Error	35	199300	5694.3	—	—	—
Total	45	266252	—	—	—	—

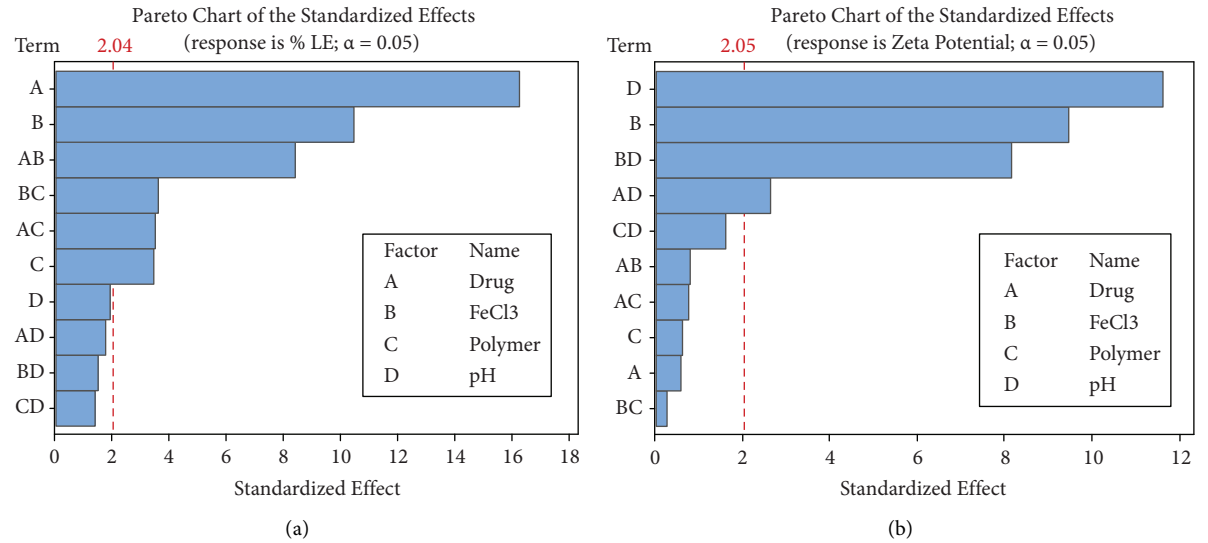

Figure 1: Continued.

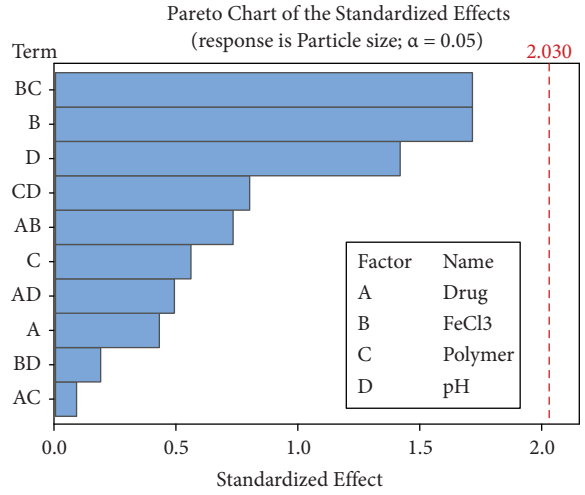

(c)

Figure 1: Pareto chart of the standardized effects on %LE (a), zeta potential (b), and particle size (c).

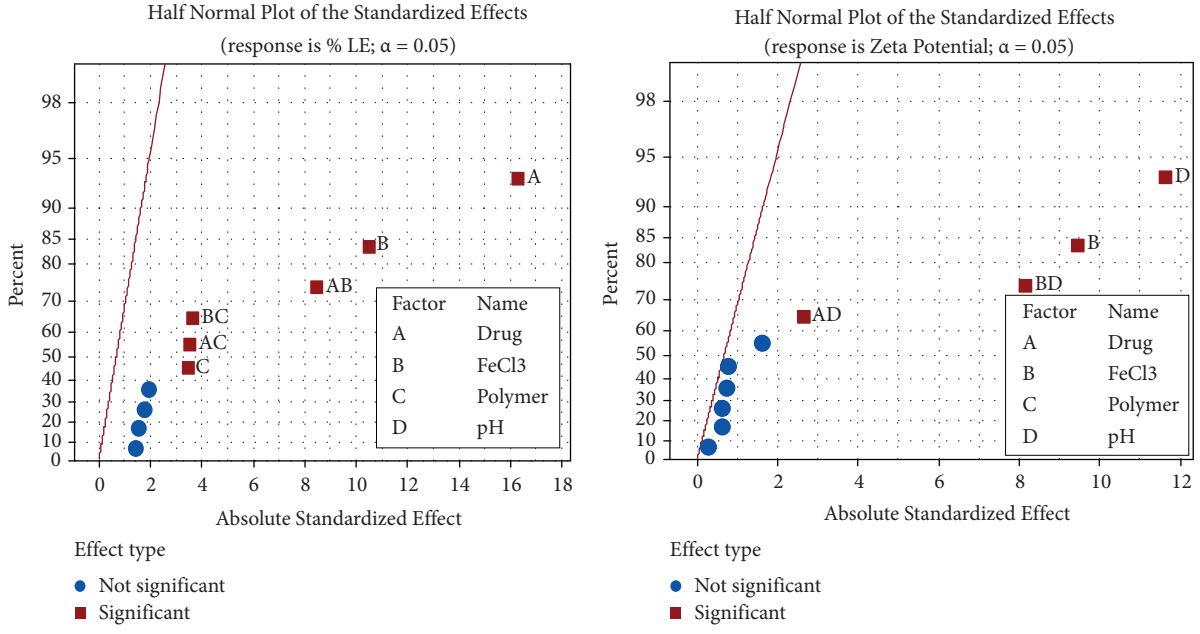

(a) (b)

Figure 2: Half normal plot for %LE (a) and zeta potential (b).

Figure 3(a) and Figure 4(a)) for %LE and zeta potential, respectively. The plot of this figure is normally distributed and resembles a straight line. There was no evidence of nonnormality and any pointing to possible outliers. Figures 3(b) and and 4(b) were observed to be within the acceptable ranges, and the histogram showed a visibly bell-shaped pattern of normal distribution.

Figures 3(c) and 4(c) clarify the residuals versus the fits plot, and Figures 3(d) and 4(d) explain the residuals versus the order plot for the %LE and zeta potential to validate the model in which residues are not dependent on each other, using a residual value versus arrangement chart. The residuals on the plot should ideally fall randomly around the centerline. The residuals were used to validate the model in which the residuals are randomly distributed and have a constant variance in the versus fits plot. Ideally, points must fall randomly on both sides. In general, these results showed that the experiment does not contain any possibility of systemic errors.

3.3.3. Contour Plot and Surface Plot of %LE and Zeta Potential e against Selected Independent Variables. Figure 5(a) shows the surface plot of %LE, where the independent variables are drug and $FeCl_3$. From the figure, the highest %LE (>45%) can be collected at a high level of drug (>0.175 gm) and a low level of $FeCl_3$ (<0.49 gm) with a fixed

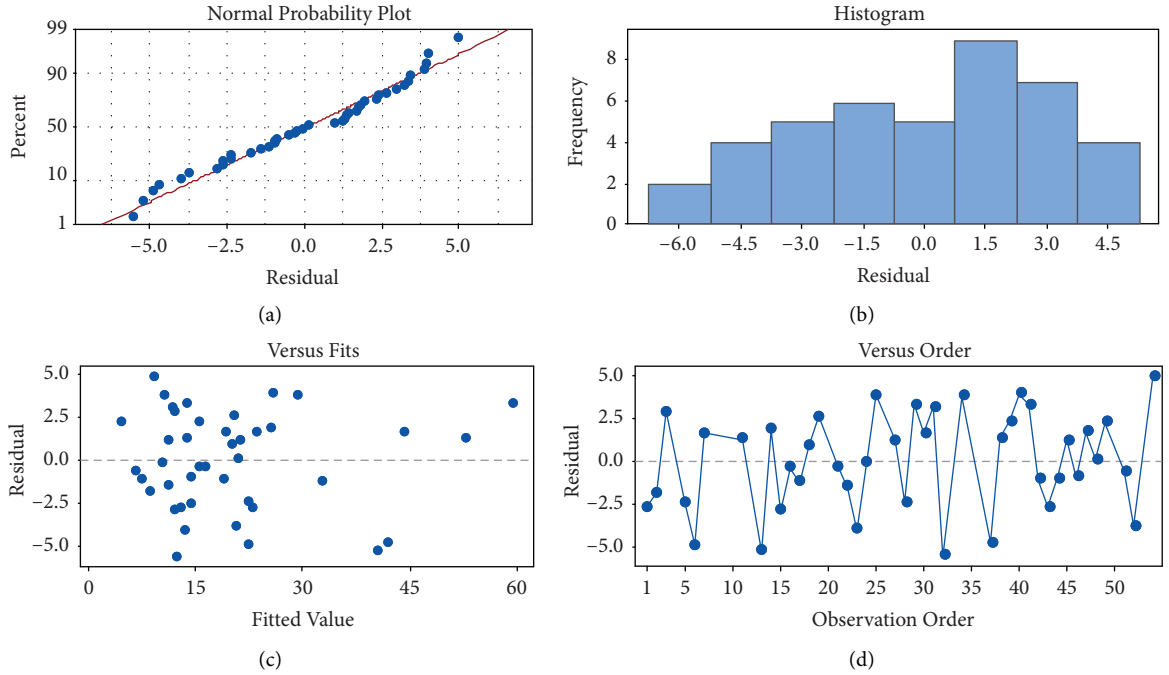

Figure 3: Residual plot for %LE. (a) Normal probablity plot; (b) histrogram; (c) versus fits; (d) versus order.

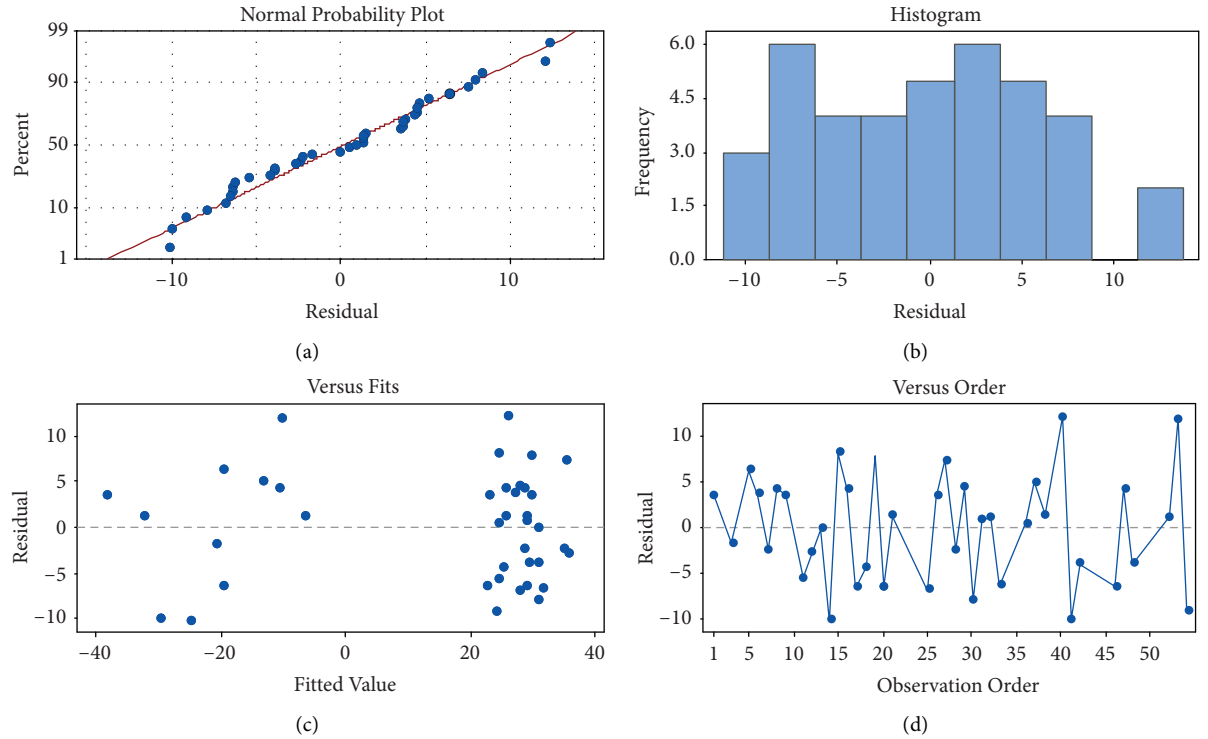

Figure 4: Residual plot for zeta potential. (a) Normal probablity plot; (b) histrogram; (c) versus fits; (d) versus order.

value of polymer (0.125 gm) and pH at 3.3 gm. These results are also shown in the contour plot in Figure 5(b).

From Figure 5(c) of the surface plot and Figure 5(d) of the contour plot of %LE, the %LE with more than 30% can be collected at a high level of drug (0.2 gm) with a large range in pH starting from 2.2 to 4.4, with a fixed value of $FeCl_3$ (0.75 gm) and polymer (0.12 gm).

The effect of the polymer and drug on the %LE is shown in Figures 5(e) and 5(f). The results show that a %LE greater than 35% can be collected by using a concentration greater

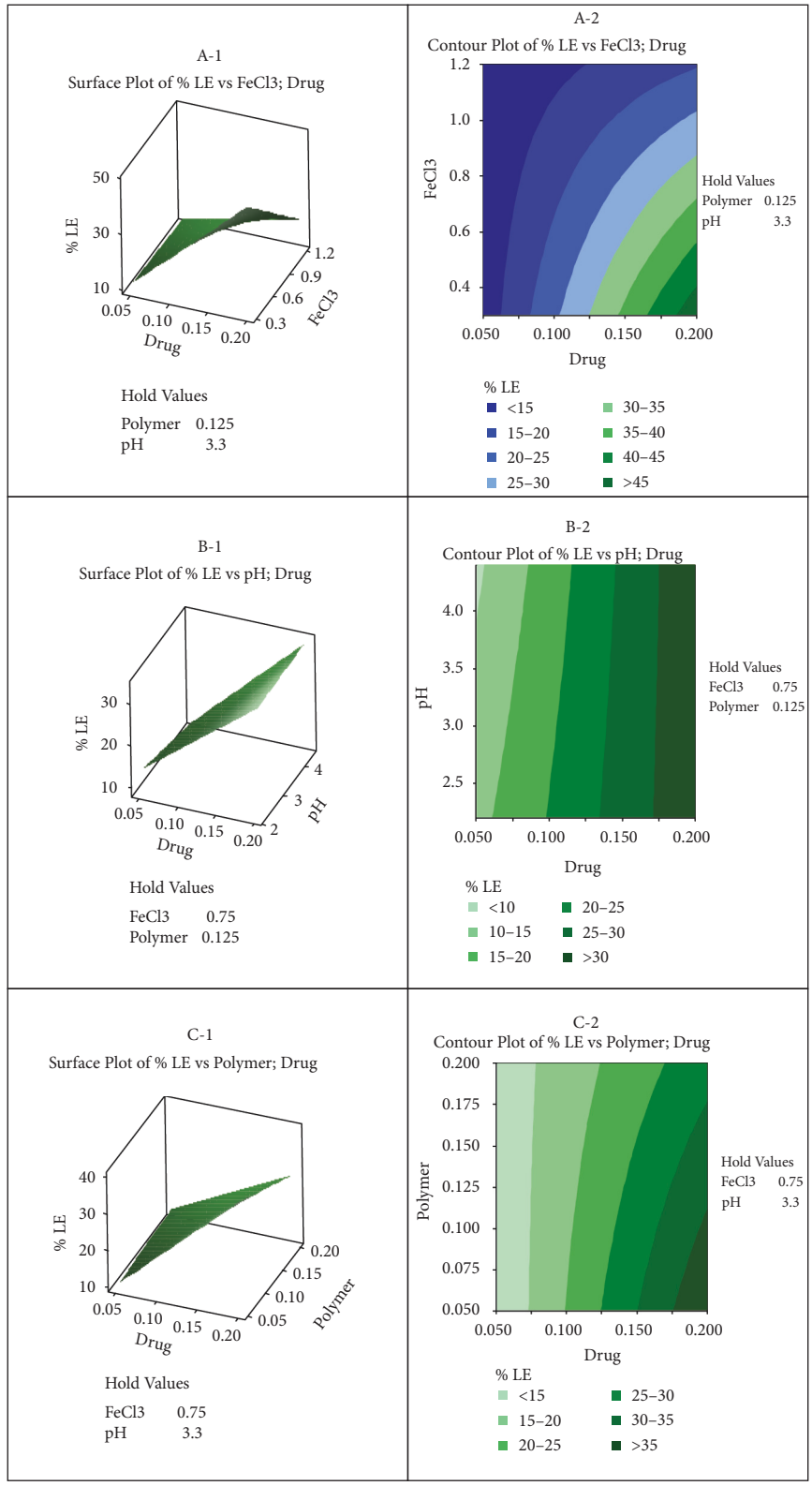

Figure 5: Continued.

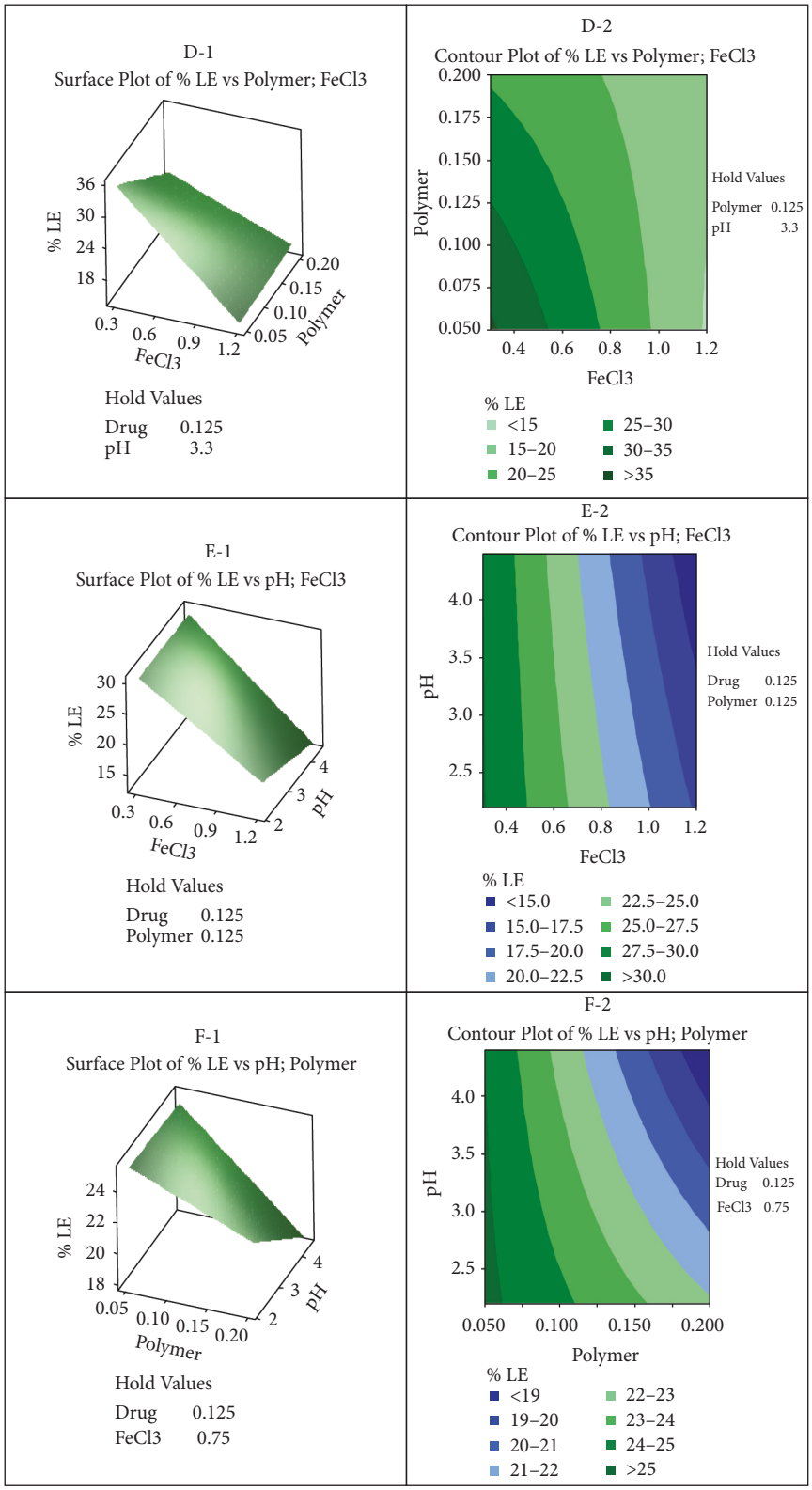

Figure 5: Contour and surface plots for %LE.

than 0.175 gm of drug and a low concentration of polymer at less than 0.1 gm, with a fixed pH (3.3) and $FeCl_3$ at 0.75 gm.

Figure 5(g) shows the surface plot of %LE, where the independent variables are polymer and $FeCl_3$. From the figure, the highest %LE (>35%) can be collected at a low level of $FeCl_3$ (<0.8 gm) and a low level of polymer (<0.125 gm) with a fixed value of drug (0.125 gm) and pH at 3.3 gm. These results are also shown in the contour plot in Figure 5(h).

From Figure 5(i) of the surface plot and Figure 5(j) of the contour plot of %LE, the %LE with more than %30 can be collected at a low level of $FeCl_3$ (<0.6 gm) with a large range in pH starting from 2.2 to 4.4, with fixed values of drug (0.125 gm) and polymer (0.125 gm).

The effect of polymer and pH on the %LE is shown in Figures 5(k) and 5(l). The results show that a %LE greater than 25% can be collected by using a concentration less than 0.100 gm of polymer with a large range in pH starting from 2.2 to 4.4, with a fixed value of drug (0.125 gm) and $FeCl_3$ at 0.75 gm.

Figure 6(a) shows the surface plot of zeta potential, where the independent variables are drug and $FeCl_3$. From the figure, the highest zeta potential (>25%) can be collected at a large scale of drug starting from 0.050 to 0200 gm and a high level of $FeCl_3$ (>0.9 gm) with a fixed value of polymer (0.125 gm) and pH at (3.3 gm). These results are also shown in the contour plot in Figure 6(b).

From Figure 6(c) of the surface plot and Figure 6(d) of the contour plot of the zeta potential, a zeta potential greater than 30% can be collected at a high level of drug (>0.159 gm) with a pH less than 2.5, with a fixed value of $FeCl_3$ (0.75) and polymer (0.125).

The effect of the polymer and drug on the zeta potential is shown in Figures 6(e) and 6(f). The results show that a zeta potential greater than 15% can be collected by using a large-scale drug starting from 0.050 to 0.200 gm, and the average scale of the polymer starts from 0.100 to 0.200 gm with a fixed pH (3.3) and $FeCl_3$ at 0.75 gm.

Figure 6(g) shows the surface plot of the zeta potential, where the independent variables are the polymer and $FeCl_3$. From the figure, the highest zeta potential (>30%) can be collected at a high level of $FeCl_3$ (>1.0 gm), and the large scale of the polymer starts from 0.05 to 0.200 gm with a fixed value of drug (0.125 gm) and pH at (3.3 gm). These results are also shown in the contour plot in Figure 6(h).

From Figure 6(i) of the surface plot and Figure 6(j) of the contour plot of the zeta potential, a zeta potential of more than 30% can be collected at a low level of $FeCl_3$ (<1.0 gm) with a large range in pH starting from 2.2 to 4.4, with fixed values of drug (0.125 gm) and polymer (0.125 gm).

The effect of the polymer and pH on the zeta potential is shown in Figures 6(k) and 6(l). The results show that a zeta potential greater than 30% can be collected by using large-scale polymers starting from 0.50 to 0.200 gm with a low pH (<2.5) and fixed values of drug (0.125 gm) and $FeCl_3$ (0.75 gm).

3.3.4. Main Effects Plot for %LE and Zeta Potential. The main effect plots are used to assess the significance of each variable at various levels, which are related to each other by line on the outcome or response.

From Figure 7(a), the %LE can reach 34% by using 0.18 gm of drug. In addition, the relation between the %LE and concentration of drug was direct. However, the relationships between %LE and $FeCl_3$, polymer, and pH were indirect. According to the figure, we can collect 30%, 25%, and 22% LE by using 0.4 gm $FeCl_3$, 0.06 gm polymer, and 2.2 PH, respectively.

From Figure 7(b), the zeta potential can reach 30% by using 1.2 g of $FeCl_3$; in addition, the relationship between the zeta potential and concentration of $FeCl_3$ was direct. However, the relationships between the zeta potential and the drug, polymer, and pH were indirect. According to the figure, we can collect 15%, 15%, and 30% zeta potentials by using 0.06 g of drug, 0.06 g of polymer, and 2.2 PH, respectively.

3.3.5. The Interaction between the Factor Effects on %LE and Zeta Potential. From Figure 8(a), the interaction between drug*PH indicates that, to prepare the nanocomposite with 32%, we should use 0.2 gm of drug at different pH values (2.2, 3.3, and 4.4). To prepare 40% LE, we used 0.2 gm of drug and 0.05 gm of polymer. In addition to preparing nanocomposites with 48% LE, we used 0.2 g of drug with 0.3 g of $FeCl_3$.

Figure 8(a) also describes the interaction between $FeCl_3$*PH and the $FeCl_3$*polymer. Based on the figure, we can prepare a nanocomposite with 30% LE at 0.4 gm $FeCl_3$ and pH 2.2, whereas, to prepare a nanocomposite with 35% LE, we should use 0.41 gm $FeCl_3$ and 0.05 polymer.

Figure 8(a) also shows the interaction between polymer*PH and the effect on %LE. Based on the figure, we can prepare 20% LE in the nanocomposite by using 0.06 mg polymer and 2.2 PH media.

From Figure 8(b), the interaction between drug*PH indicates that, to prepare nanocomposites with 22%, we should use 0.2 gm of drug at different pH values (2.2). If the lines are parallel to the drug with $FeCl_3$, the plot shows that there is no interaction between these two factors, and if the lines are parallel to the drug with polymer, the plot shows that there is no interaction between these two factors.

Figure 8(b) also describes the interaction between $FeCl_3$*PH and the $FeCl_3$*polymer. Based on the figure, we can prepare nanocomposites with 20% zeta potential at 1.2 gm $FeCl_3$ at different pH values (2.2, 3.3, and 4.4), whereas, to prepare nanocomposites with 30% zeta potential, we should use 1.2 gm $FeCl_3$ and 0.05 polymer.

Figure 8(b) also shows the interaction between polymer*PH and the effect on the zeta potential. Based on the figure, we can prepare a 30% zeta potential nanocomposite by using 0.2 mg polymer and 2.2 PH media.

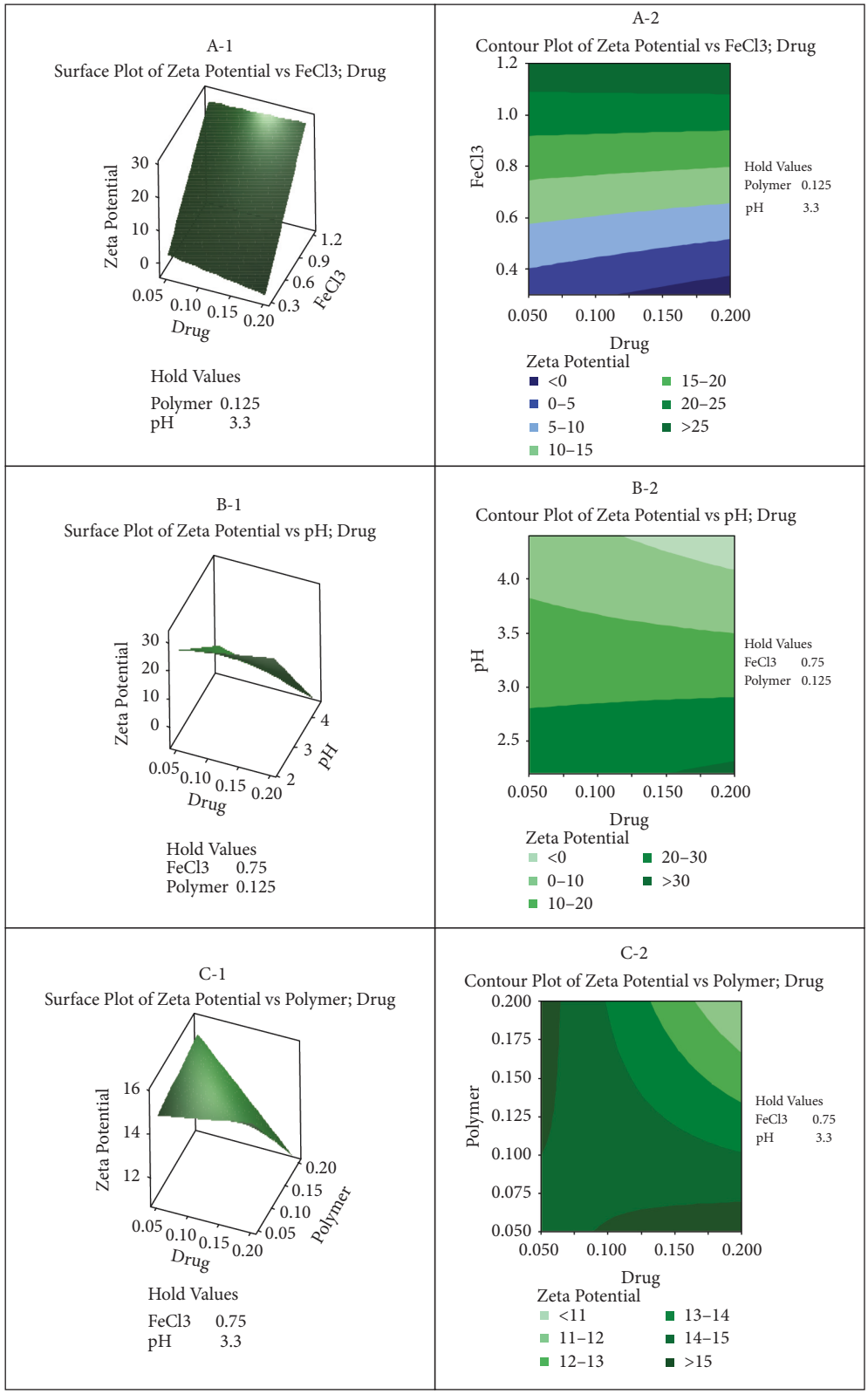

Figure 6: Continued.

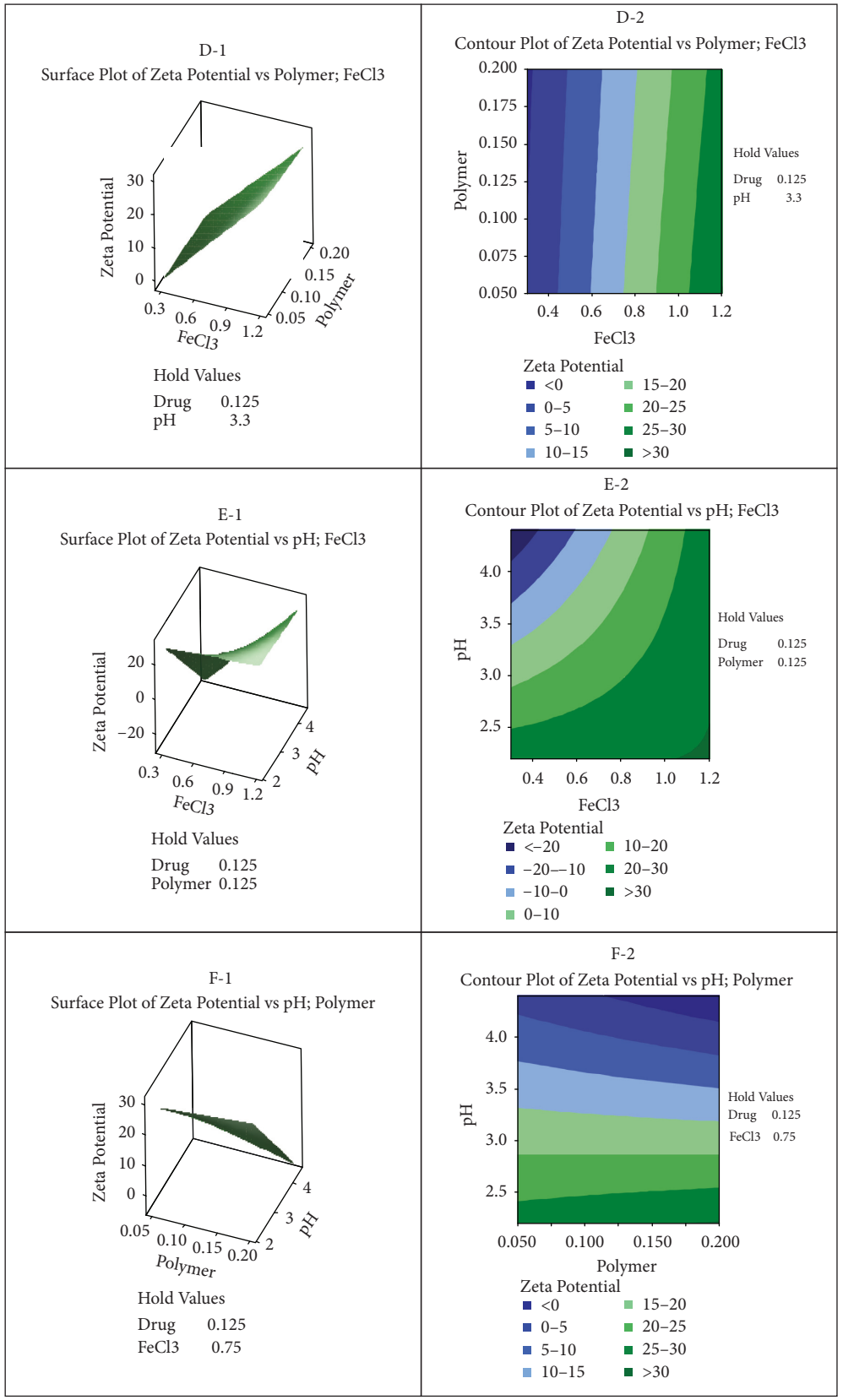

Figure 6: Contour and surface plots for zeta potential.

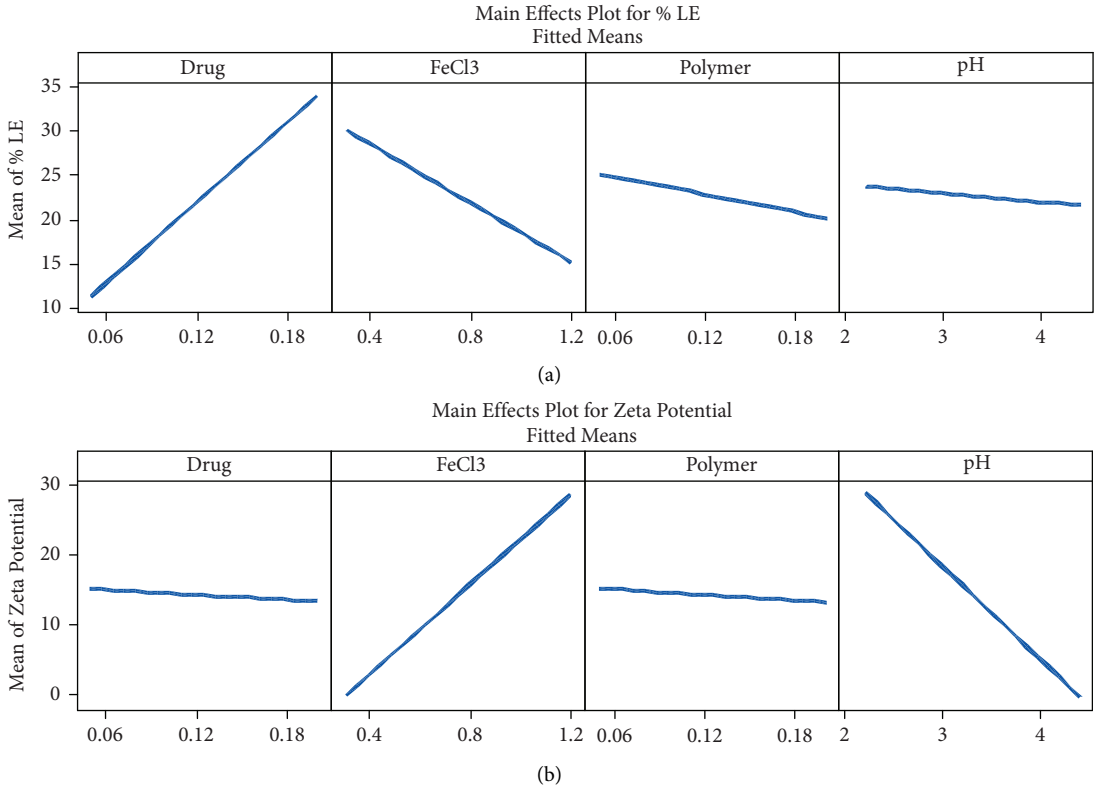

Figure 7: Main effects plot for %LE (a) and zeta potential (b).

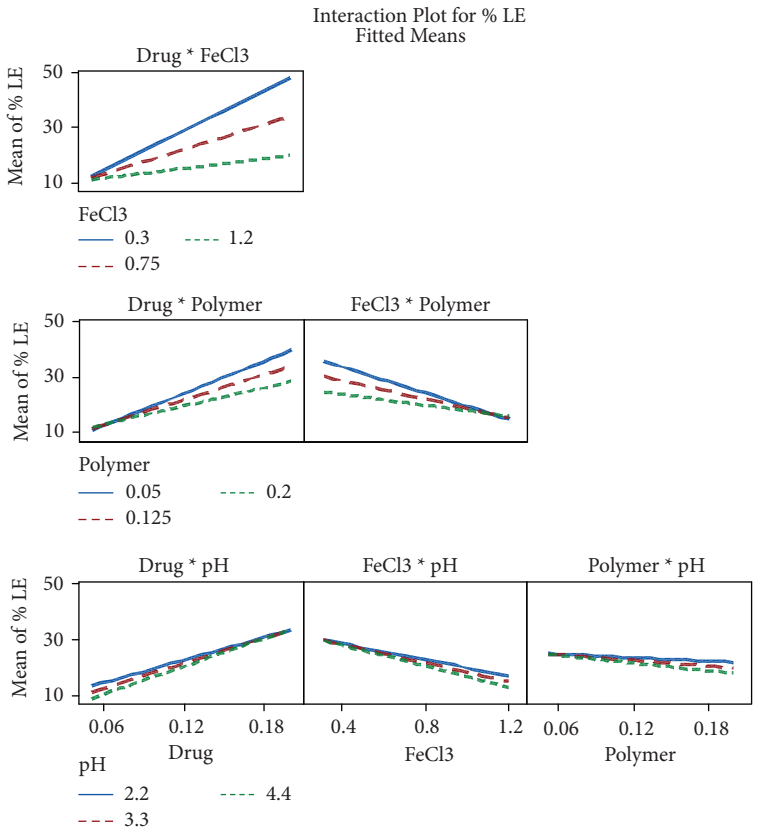

(a)

Figure 8: Continued.

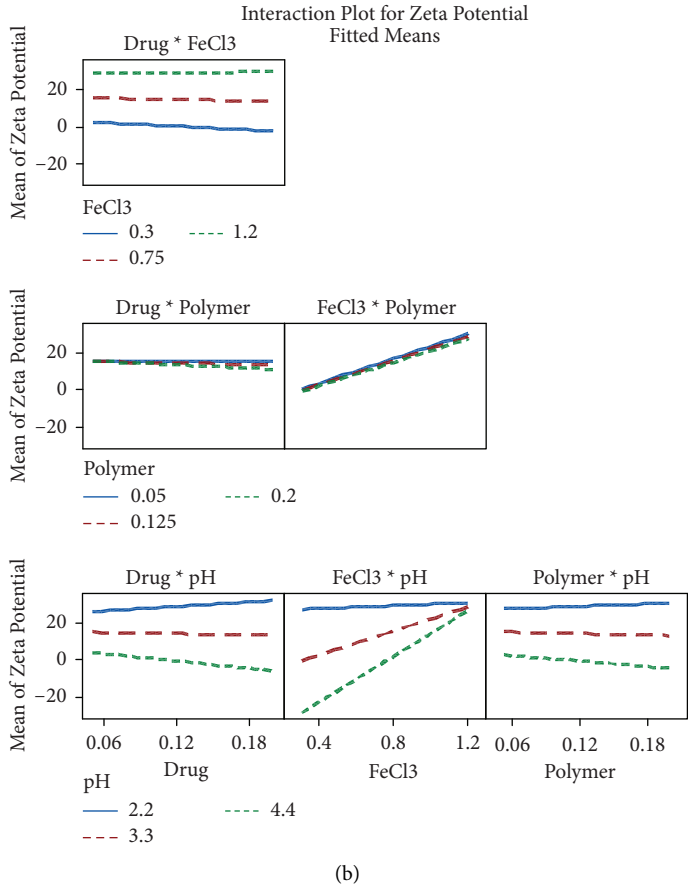

(b)

Figure 8: Interaction plot for LE% (a) and zeta potential (b).

3.4. Optimization and Validation of %LE and Zeta Potential

3.4.1. Optimization of %LE and Zeta Potential. Figure 9 shows an optimized concentration for the response factors %LE and zeta potential. The first optimized compound selected had the highest %LE and the highest Zeta potential.

The second and third optimized samples were collected randomly by changing the vertical red line in Figure 9.

3.4.2. Validation of %LE and Zeta Potential. According to the optimized nanocomposite, the other two samples in Figure 9 contain three independent variables with the predicate %LE and zeta potential. These three samples were prepared in the lab, and, after that, we deferred the %LE and zeta potential.

From Table 8, we can see that the bias for the first formula was approximately 5.3% and 14.6% (drug = 0.2, $FeCl_3$ = 0.3, polymer = 0.05, and pH = 2.2) for %LE and zeta potential, respectively. In addition, the bias for the second formula was approximately −5.2% and −13.1% for %LE and zeta potential, respectively (drug = 0.121, $FeCl_3$ = 0.6926, polymer = 0.12, and pH = 3.1) and the bias for the third formula was approximately −4.1% and −19.0% for %LE and zeta potential, respectively (drug = 0.2, $FeCl_3$ = 0.3, polymer = 0.2, and pH = 2.2). These findings and information supported the validity of the model created and indicated good correlation between experimental and predicted values. A bias formula was developed under optimized factors to compare experimental values with the predictor values.

3.5. Characterizations of the Optimized Nanocomposite

3.5.1. X-Ray Diffraction (XRD). Powder XRD patterns of polymer nanoparticles and cromolyn-polymer nanocomposites are presented in Figures 10(a) and 10(b), respectively. From Figure 10(a), the strong peaks at $2\theta = 31.7^{\circ}$ and 45.3° indicate semicrystalline properties. In addition, the cromolyn-polymer nanocomposite in Figure 10(b) shows a peak similar to that of polymer nanoparticles. From the literature, free cromolyn shows different sharp peaks at 2Θ 8, 9.8, 11.5, 14, 16.9, 19.7, 24.3, and 26.6, indicating that cromolyn is highly crystalline in nature [20].

In addition, the absence of characteristic drug peaks in the nanocomposite shown in Figure 1(b) indicated that the drug had converted from a crystalline into an amorphous form and was incorporated into the polymer.

3.5.2. Fourier Transform Infrared (FTIR) Spectroscopy. Figures 11(a)–11(d) show FTIR spectra for cromolyn, polymer, polymer nanoparticle, and nanocomposite, respectively. From the figures, pure cromolyn showed basic

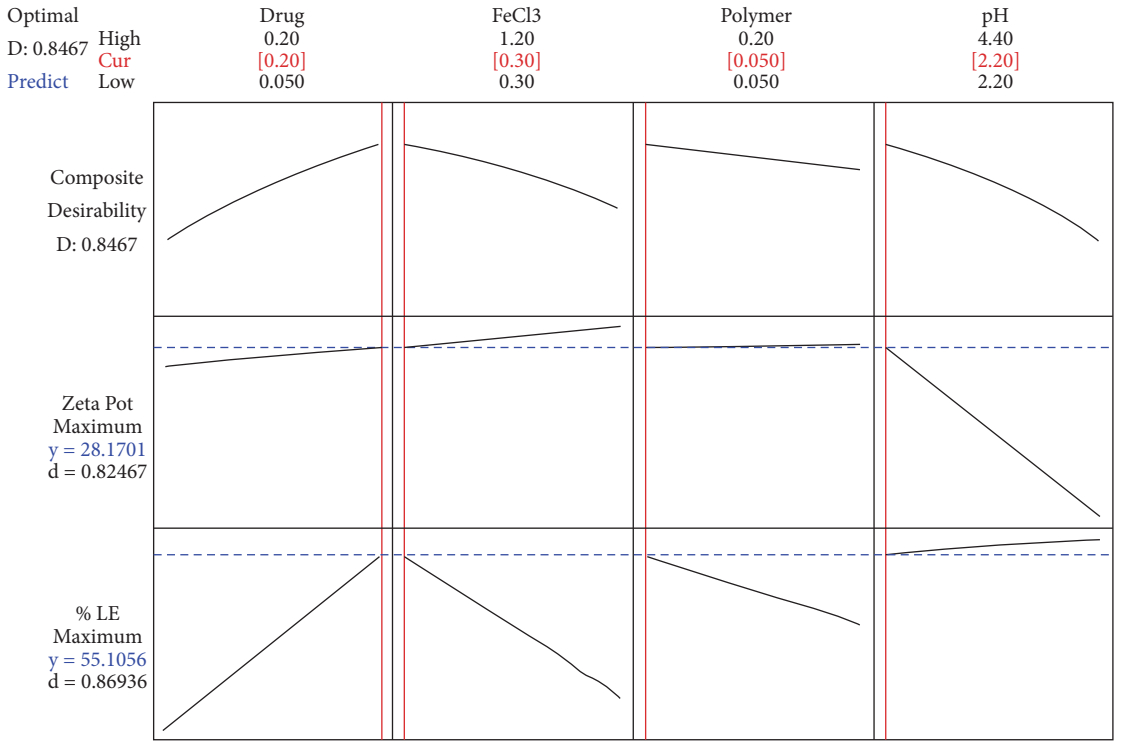

Figure 9: Response optimization plot for different responses.

Table 8: Comparative results between observed and predicted response values of variables of optimized formulation.

Concentrations	Experimental response	Predicted values	Observed values	Bias (%)
Drug (0.2 gm) $FeCl_3$ (0.3 gm) Polymer (0.05 gm) pH = 2.2	LE (%)	55.1%	58.0%	5.3%
	Zeta potential (mV)	28.1 mV	32.2 mV	14.6%
Drug (0.121 gm) $FeCl_3$ (0.6926 gm) Polymer (0.121 gm) pH = 3.1	LE (%)	23.2%	22.0%	−5.2%
	Zeta potential (mV)	15.3 mV	13.3 mV	−13.1%
Drug (0.2 gm) $FeCl_3$ (0.3 gm) Polymer (0.2 gm) pH = 2.2	LE (%)	39.3%	37.7%	−4.1%
	Zeta potential (mV)	29.5 mV	23.9 mV	−19.0%

% bias was calculated as (observed value − predicted value/predicted value) ×100

peaks at 1605 cm^{-1} due to (C=O), a broad band at 3285 cm^{-1} due to (O-H) stretching vibrations, and characteristic peaks at 2880 cm^{-1} due to (C-H alkane). An aromatic C-H gives bands at 1477 cm^{-1}, 1573 cm^{-1}, and 1410 cm^{-1} (asymmetric and symmetric COO^-) and a large number of characteristic absorption bands in the fingerprint region (1400–600 cm^{-1}) [21].

The IR spectra of the polymer are shown in Figure 11(b). The stretching vibrations of the carboxylic and carbonyl groups ranged from 1720 to 1727 cm^{-1}, and the formation of hydrogen bonding carboxylic acid O-H stretching appeared as a very broad band from 2543 to 3623 cm^{-1}. In the range of 3732 to 3737 cm^{-1}, a weak band for the monomeric O-H stretch band was also observed. From 1626 to 1636 cm^{-1}, strong bands of the stretching vibration for the carbonyl bond of the amide group were observed. The IR band of amide group NH bonds was observed for stretching and bending vibrations between 3268 and 3316 cm^{-1}1 and between 1517 and 1527 cm^{-1}, respectively [22].

The IR spectra of blank-polymer nanoparticles are shown in Figure 11(c). The spectrum of the polymer nanoparticles showed a characteristic vibrational peak for O-H at 3320 cm^{-1}. The peak observed at approximately 583 cm^{-1} is characteristic of Fe vibrations. Comparing the spectrum of the nanocomposite with the spectrum of the blank-polymer particle, specific peaks of cromolyn appeared at 1604 cm^{-1} due to C=O, and a band at approximately 1477 cm^{-1} was also observed due to aromatic C-H. All these

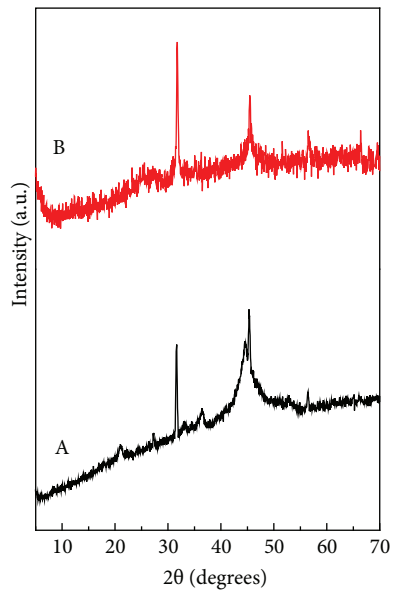

Figure 10: Powder X-ray diffraction patterns of the polymer nanoparticles (a) and cromolyn-polymer nanocomposite (b).

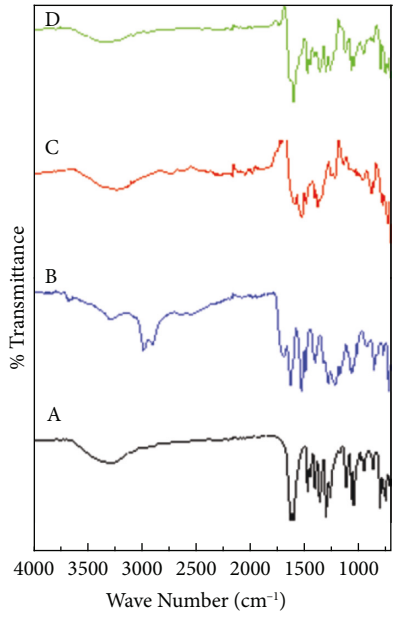

Figure 11: FTIR of the cromolyn (a), polymer (b), polymer nanoparticle (c), and nanocomposite (d).

results indicate the incorporation of cromolyn into the nanocomposite, as shown in Figure 11(d).

3.5.3. Scanning Electron Microscopy (SEM). The surface morphology of the samples for polymer nanoparticles and nanocomposites as studied by scanning electron microscopy (FE-SEM) is shown in Figures 12(a)and 12(b), respectively. Figure 12 shows a spherical shape and nearly uniform size with diameters of 55 and 68 nm for the polymer nanoparticles and nanocomposites, respectively.

3.5.4. In Vitro Release Study. The in vitro release of cromolyn from the cromolyn-polymer nanocomposite at pH 7.4 is shown in Figure 13. It is shown that the amount of cromolyn released at 23 hours was 100%. Cromolyn is released via several mechanisms, such as diffusion, erosion, and swelling. In the diffusion method, the drug diffuses from the matrix of the polymer to the surrounding area. In the erosion method, the polymer breaks the bond and then releases the drug.

The medium's pH value, surrounding media enzymes, and uptake of water via the polymer can all affect drug

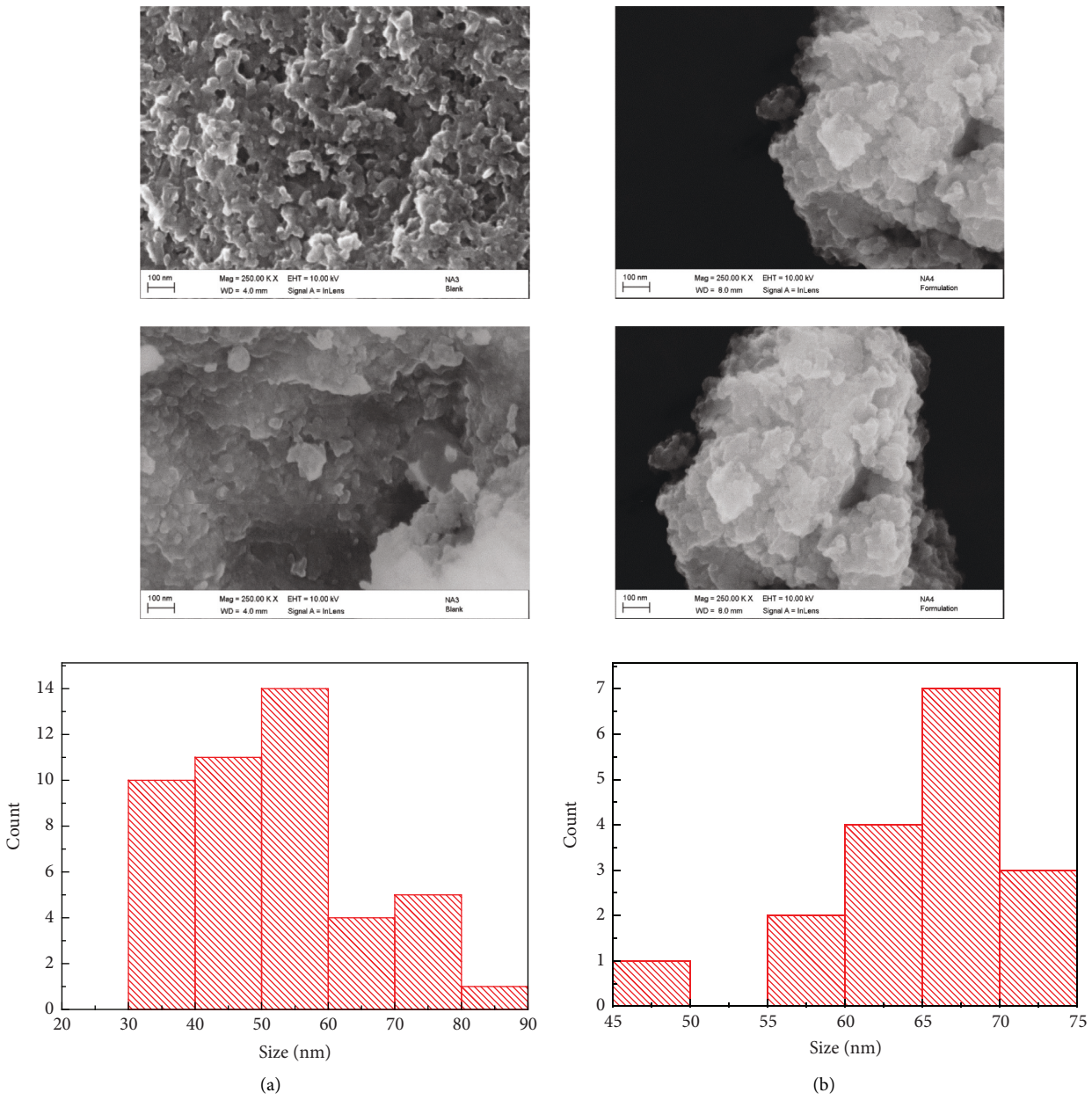

Figure 12: Scanning electron microscope images of polymer nanoparticles (a) and polymer nanocomposites (b).

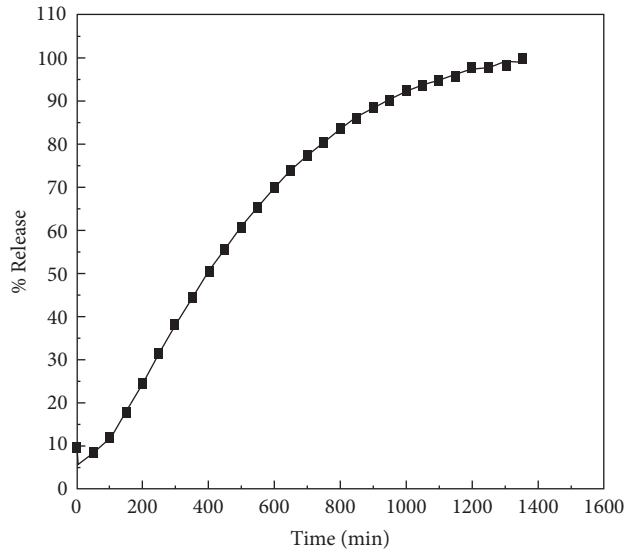

Figure 13: In vitro release profile of cromolyn from the cromolyn-polymer nanocomposite.

release. The swelling of hydrogel beads is one of the main mechanisms that play an important role in drug release by allowing water to enter through the polymer and dissolve it.

4. Conclusion

In this study, the main aim was to use polyamide-disulfide nanoparticles as a drug delivery system. We used cromolyn as a model and formed nanocomposites. In this work, we investigated the effect of independent variables (cromolyn, $FeCl_3$, polymer, and pH) on the dependent variable (%LE, zeta potential, and particle size). We used Minitab 18 software to evaluate the nanocomposite. The study obtained % LE (25%–45%) and zeta potential (15%–30%). The formulation that we prepared can be used as a drug delivery system for cromolyn to improve its absorption, stability, bioavailability, and drug release profile for extended release for 23 hours. This study indicated that cromolyn with the polymer had the most significant impact on %LE and zeta potential.

Data Availability

The data are available upon request from Professor Samer Hasan Ahmad Hussein-Al-Ali (e-mail: sameralali72@yahoo.com or samer.alali@iu.edu.jo).

Conflicts of Interest

The authors report that there are no conflicts of interest in this work.

Acknowledgments

The authors would like to thank the Faculty of Pharmacy at Isra University for providing funding for this research under grant no. 2020/2021/4–23. Also, the authors would like to acknowledge the Institute of Functional Nanosystems for the permission to use their advanced facilities in UIM University (Germany).

References

[1] A. Cappy, D. Stievenard, and D. Vuillaume, "Nanotechnology: the next industrial revolution?" in *Gallium Arsenide Applications Symposium*, pp. 1–4, 2002.

[2] S. A. Agnihotri, N. N. Mallikarjuna, and T. M. Aminabhavi, "Recent advances on chitosan-based micro-and nanoparticles in drug delivery," *Journal of Controlled Release*, vol. 100, no. 1, pp. 5–28, 2004.

[3] T. Yih and M. Al-Fandi, "Engineered nanoparticles as precise drug delivery systems," *Journal of Cellular Biochemistry*, vol. 97, no. 6, pp. 1184–1190, 2006.

[4] S. Gelperina, K. Kisich, M. D. Iseman, and L. Heifets, "The potential advantages of nanoparticle drug delivery systems in chemotherapy of tuberculosis," *American Journal of Respiratory and Critical Care Medicine*, vol. 172, no. 12, pp. 1487–1490, 2005.

[5] S.-D. Li and L. Huang, "Pharmacokinetics and biodistribution of nanoparticles," *Molecular Pharmaceutics*, vol. 5, no. 4, pp. 496–504, 2008.

[6] D. K. Ali, A. M. Al-Zuheiri, and B. A. Sweileh, "pH and reduction sensitive bio-based polyamides derived from renewable dicarboxylic acid monomers and cystine amino acid," *International Journal of Polymer Analysis and Characterization*, vol. 22, no. 4, pp. 361–373, 2017.

[7] S. Murphy, "Cromolyn sodium: basic mechanisms and clinical usage," *Pediatric Asthma, Allergy and Immunology*, vol. 2, no. 4, pp. 237–254, 1988.

[8] S. Yasmeen, S. Khatun, F. A. Qais, and F. Abul Qais, "Characterization of interactions between cromolyn sodium and bovine serum albumin by spectroscopic, calorimetric and computational methods," *Journal of Biomolecular Structure and Dynamics*, vol. 38, no. 3, pp. 722–732, 2019.

[9] A. W. G. Alani and J. R. Robinson, "Mechanistic understanding of oral drug absorption enhancement of cromolyn sodium by an amino acid derivative," *Pharmaceutical Research*, vol. 25, no. 1, pp. 48–54, 2008.

[10] R. N. Brogden, T. M. Speight, and G. S. Avery, "Sodium cromoglycate (cromolyn sodium): a review of its mode of action, pharmacology, therapeutic efficacy and use," *Drugs*, vol. 7, no. 3, pp. 164–282, 1974.

[11] W. B. Liechty, D. R. Kryscio, B. V. Slaughter, and N. A. Peppas, "Polymers for drug delivery systems," *Annual Review of Chemical and Biomolecular Engineering*, vol. 1, pp. 149–173, 2010.

[12] I. Rodriguez, J. Flores Bello, J. Marie Serrano Valcarcel, and V. Lopez-Mejias, "Design of potential pharmaceutical-based metal complexes derived from cromolyn a mast cell stabilizer," *ACS Omega*, vol. 5, no. 46, pp. 29714–29721, 2020.

[13] P. Sacco, S. Pedroso-Santana, Y. Kumar, N. Joly, P. Martin, and P. Bocchetta, "Ionotropic gelation of chitosan flat structures and potential applications," *Molecules*, vol. 26, no. 3, p. 660, 2021.

[14] S. Pedroso-Santana and N. Fleitas-Salazar, "Ionotropic gelation method in the synthesis of nanoparticles/microparticles for biomedical purposes," *Polymer International*, vol. 69, no. 5, pp. 443–447, 2020.

[15] H. A. K. Sabbagh, S. H. Hussein-Al-Ali, M. Z. Hussein, Z. Abudayeh, R. Ayoub, and S. M. Abudoleh, "A statistical study on the development of metronidazole-chitosan-alginate

nanocomposite formulation using the full factorial design," *Polymers*, vol. 12, no. 4, p. 772, 2020.

[16] I. Kuncahyo, S. Choiri, A. Fudholi, R. Martien, and A. Rohman, "Assessment of fractional factorial design for the selection and screening of appropriate components of a self-nanoemulsifying drug delivery system formulation," *Advanced Pharmaceutical Bulletin*, vol. 9, no. 4, pp. 609–618, 2019.

[17] N. Subramanian, A. Yajnik, and R. S. R. Murthy, "Artificial neural network as an alternative to multiple regression analysis in optimizing formulation parmaeters of cytarabine liposomes," *AAPS PharmSciTech*, vol. 5, no. 1, pp. 11–19, 2004.

[18] S. H. Hussein-Al-Ali, S. M. Abudoleh, Q. I. A. Abualassal, Z. Abudayeh, Y. Aldalahmah, and M. Z. Hussein, "Preparation and characterisation of ciprofloxacin-loaded silver nanoparticles for drug delivery," *IET Nanobiotechnology*, vol. 16, no. 3, pp. 92–101, 2022.

[19] S. H. Hussein-Al-Ali, M. Zobir, R. Ayoub, S. Fakurazi, Q. Abualassal, and Y. Al-Dalahmeh, "Development of new drug formulations: cetirizine-polymers nanoparticles," *Acta Poloniae Pharmaceutica—Drug Research*, vol. 78, no. 3, pp. 385–398, 2021.

[20] R. R. Patel, G. Khan, S. Chaurasia, N. Kumar, and B. Mishra, "Rationally developed core–shell polymeric-lipid hybrid nanoparticles as a delivery vehicle for cromolyn sodium: implications of lipid envelop on in vitro and in vivo behaviour of nanoparticles upon oral administration," *RSC Advances*, vol. 5, no. 93, pp. 76491–76506, 2015.

[21] R. R. Patel, S. Chaurasia, G. Khan, P. Chaubey, N. Kumar, and B. Mishra, "Cromolyn sodium encapsulated PLGA nanoparticles: an attempt to improve intestinal permeation," *International Journal of Biological Macromolecules*, vol. 83, pp. 249–258, 2016.

[22] G. Lawrie, I. Keen, B. Drew et al., "Interactions between alginate and chitosan biopolymers characterized using FTIR and XPS," *Biomacromolecules*, vol. 8, no. 8, pp. 2533–2541, 2007.

Hindawi
Journal of Chemistry
Volume 2021, Article ID 4942659, 13 pages
https://doi.org/10.1155/2021/4942659

Research Article

Development, Optimization, and Evaluation of Luliconazole Nanoemulgel for the Treatment of Fungal Infection

Nabil A. Alhakamy,[1,2,3] Shadab Md,[1,2,3] Md Shoaib Alam,[4] Rasheed A. Shaik,[5] Javed Ahmad,[6] Abrar Ahmad,[7] Hussam I. Kutbi,[8] Ahmad O. Noor,[8] Alaa Bagalagel,[8] Douha F. Bannan,[8] Bapi Gorain,[9,10] and Ponnurengam Malliappan Sivakumar[11]

[1]*Department of Pharmaceutics, Faculty of Pharmacy, King Abdulaziz University, Jeddah 21589, Saudi Arabia*
[2]*Center of Excellence for Drug Research & Pharmaceutical Industries, King Abdulaziz University, Jeddah 21589, Saudi Arabia*
[3]*Mohamed Saeed Tamer Chair for Pharmaceutical Industries, King Abdulaziz University, Jeddah 21589, Saudi Arabia*
[4]*Research & Development, Jamjoom Pharmaceuticals, Jeddah 21442, Saudi Arabia*
[5]*Department of Pharmacology & Toxicology, Faculty of Pharmacy, King Abdulaziz University, Jeddah 21589, Saudi Arabia*
[6]*Department of Pharmaceutics, College of Pharmacy, Najran University, Najran, Saudi Arabia*
[7]*Department of Biochemistry, Faculty of Sciences, King Abdulaziz University, Jeddah 21589, Saudi Arabia*
[8]*Department of Pharmacy Practice, Faculty of Pharmacy, King Abdulaziz University, Jeddah, Saudi Arabia*
[9]*School of Pharmacy, Faculty of Health and Medical Sciences, Taylor's University, Subang Jaya 47500, Selangor, Malaysia*
[10]*Centre for Drug Delivery and Molecular Pharmacology, Faculty of Health and Medical Sciences, Taylor's University, Subang Jaya, Selangor, Malaysia*
[11]*Sabanci University Nanotechnology Research and Application Center (SUNUM), Tuzla 34956, Istanbul, Turkey*

Correspondence should be addressed to Shadab Md; shadabmd1982@gmail.com and Ponnurengam Malliappan Sivakumar; sivamedchem@gmail.com

Received 6 June 2021; Accepted 16 October 2021; Published 5 November 2021

Academic Editor: Bijan Das

The present study aimed to optimize luliconazole nanoemulsion using Box–Behnken statistical design, which was further incorporated into the polymeric gel of Carbopol 934. The formulation was characterized for its size, entrapment efficiency, *ex vivo* permeation, and mechanism of release. The size of the dispersed globules of the optimized drug-loaded nanoemulsion was found to be 17 ± 3.67 nm with a polydispersity index (PDI) less than 0.5. Although the surface charge was recorded at −9.53 ± 0.251, the stability was maintained by the polymeric matrix that prevented aggregation and coalescence of the dispersed globules. The luliconazole-nanoemulgel (LUL-NEG) was characterized for drug content analysis, viscosity, pH, and refractive index, where the results were found to be 99.06 ± 0.59%, 9.26 ± 0.08 Pa.s, 5.65 ± 0.17, and 1.31 ± 0.08, respectively. The permeation across the rat skin was found to be significantly higher with LUL-NEG when compared with LUL gel. Furthermore, the skin irritation test performed in experimental animals revealed that the blank NEG, as well as the LUL-NEG, did not produce any signs of erythema following 48 h exposure. In addition, the histopathological findings of the experimental skins reported no abnormal signs at the formulation application site. Finally, the NEG formulation was found to create a statistically significant zone of inhibition ($P < 0.05$) when compared to all other test groups. Overall, it could be summarized that the nanoemulgel approach of delivering luliconazole across the skin to treat skin fungal infections could be a promising strategy.

1. Introduction

Luliconazole (LUL), an antifungal drug containing imidazole moiety with ketone dithioacetate, is a broad-spectrum agent, which has shown its potential against wide varieties of fungi, especially against filamentous fungi, for example, dermatophytes [1]. Although the exact mechanism of this novel agent for antifungal efficacy is unknown, it has been reported that LUL acts by inhibiting the fungal cytochrome P450; that is, 14-α demethylase enzyme thus prevents the

biosynthesis of ergosterol from lanosterol and interrupts cell wall synthesis within the fungi [2–4]. Since 2013, the United States Food and Drug Administration has approved the commercial cream formulation of LUL (1%, w/w) for clinical use against fungal infections and dermatophytosis including tinea corporis, tinea cruris, and tinea pedis resulting from the invasion of *Epidermophyton floccosum* and *Trichophyton rubrum* [5]. The solubility of LUL is low. This low solubility restricts permeation of the drug across the skin upon topical delivery [6]. Alternatively, conventional topical cream formulations possess several drawbacks of low permeation from the stratum corneum along with reduced retention at the site of application [7]. Moreover, the rate-limiting step for LUL permeation is its solubility in the lipid phase of the stratum corneum that limits its dermal availability [6]. With no formulations in the market other than cream and lotion for LUL, there is an urgent requirement for novel deliveries for improved retention and penetration from the site of skin application. A few research outcomes are available in the literature where different researchers tried to improve the delivery approach of LUL via liposomal and ethosomal gel preparation [7], lyotropic liquid crystalline nanoparticle [8], nanocrystals-loaded hydrogel [6], niosomal gel [9], solid lipid nanoparticle gel [10], and so on. The ethosomal and elastic liposomal-based gel preparation of LUL had reported safety and efficacy of the formulation without delivering the drug to the systemic circulation [7]. Similarly, 181 ± 12.3 nm particle size of the LUL lyotropic liquid crystalline nanoparticle increased retention of the drug (LUL) on the stratum corneum and epidermis when compared with the commercial topical formulation. This increased retention time allowed the formulation to penetrate higher in the different layers of the skin [8]. An alternate formulation approach by Kumar and team depicted that nanocrystals-loaded hydrogel of LUL could retain highest in different skin layers when compared to the coarse suspension, nanosuspension, and D-gel [6]. Although extensive research was not conducted, it was concluded by Garg and team that the niosomal gel formulation of LUL could provide a platform for topical delivery against *Candida* [9]. Alternatively, topical gel delivery of LUL solid lipid nanoparticle showcased safety as there were no signs of oedema and erythema [10]. The advantages of different formulation approach on topical delivery of LUL have been implemented in this research via the development of nanoemulgel (NEG) delivery approach.

Advancement of NEG-based researches in the recent era has gained tremendous attention because of their stability, appearance, penetrability across the biological membranes, longer retention, and sustained release profile of the entrapped drug [11–14]. NEG is a novel biphasic polymeric nanoemulsion platform to topically deliver lipophilic agents, where nanometric size range of the oil globules facilitates permeation across the stratum corneum of the skin [11]. The polymeric networks in this architecture allow entrapping the dispersed globules promoting the stability of the formulation following incorporation of lipidic agents within the oil core of oil-in-water nanoemulsion. This NEG platform possesses the potential of enhanced solubility of lipophilic drugs, sustained release of the entrapped therapeutic agents, superior topical applicability, biocompatibility, and biodegradability [15, 16]. The thixotropic NEG allows easy spreadability at the desired site and prolongs retention at the application site due to mucoadhesive property, where the hydrophilic nature of the formulation allows easy removal from the application site after accomplishment of desired efficacy [16, 17]. A wide number of researches have been conducted with NEG-based topical formulations of lipophilic drugs for improved efficacy of the entrapped therapeutics [15, 18, 19].

Thus, the present study was attempted to develop and optimize LUL-loaded nanoemulgel for improved efficacy against fungal infection by enhancing the solubility and simultaneously the permeability across the skin barrier. Eucalyptus oil was selected as the lipid phase in the preparation of the nanoemulsion containing LUL for our study. This eucalyptus oil has been well documented for its antifungal efficacy [20, 21]. Thus, it is hypothesized that the final NEG formulation of LUL would provide improved antifungal efficacy. The development of nanoemulsion was optimized using Box–Behnken statistical design and characterized. Furthermore, the permeation across the rat skin, zone of inhibition against *Candida*, and the skin irritability tests were performed to establish the superiority of the LUL-NEG over commercial preparation.

2. Materials and Methods

2.1. Materials. Luliconazole (purity >98%) was provided as a gift sample from Jamjoom Pharmaceutical, Jeddah, Saudi Arabia, whereas eucalyptus oil was obtained from Allin Exporters, Noida, India. Carbopol 934, Tween 20, and polyethylene glycol 200 (PEG 200) were purchased from Sigma Aldrich, MO, USA. The HPLC grade solvents were purchased from Merck, NJ, USA. The rest of the chemicals used in this current experiment were of analytical grade.

2.2. Preparation of Nanoemulsion. The selection of surfactant for the development of eucalyptus oil nanoemulsion was made based on the literature [22]. The selection of cosurfactant was made on the pseudoternary phase diagram, and finally, the ratio of surfactant and cosurfactant was done following evaluation of a wide range (4 : 1, 3 : 1, 2 : 1, 1 : 1, 1 : 2, 1 : 2, 1 : 3, and 1 : 4) [23]. A preliminary study on the solubility of LUL was analysed in eucalyptus oil, surfactant (Tween 20), and PEG 200 (selected cosurfactant) to determine the maximum drug solubility within different components of nanoemulsion [24].

The formulation was developed following solubilization of the drug into the oil phase and mixed using a vortex mixer for 10 min. The mixture of surfactant and cosurfactant (Smix) was then added to the drug solution in the oil followed by the addition of aqueous phase and high-speed homogenization (6000 rpm) using Ultra Turrax® equipment (IKA, Germany) for 15 min under an ice bath to control the temperature. Finally, a clear transparent homogenous nanoemulsion was developed.

2.3. Optimization of Nanoemulsion by Box–Behnken Statistical Design. Optimization of % of oil, Smix, and stirring time for the nanoemulsion development was achieved using Box–Behnken statistical design (Design Expert®, version 12; State-Ease Inc., USA). In the optimization process, three independent variables (percentage of oil, Smix, and homogenization time) were considered as three factors and the effect of their interaction at their three levels (–1, 0, and 1) on globule size and entrapment efficiency of the formulation was studied. The software suggested 17 batches of formulations with varying levels of three independent variables. The formulations were developed and the globule size and entrapment efficiency for all the 17 batches were determined following the methodology mentioned in Sections 2.4 and 2.5. The data were incorporated in the response column in the software to obtain the optimized formation. Statistical analysis was performed using analysis of variance (ANOVA) and the effect of the interaction of three independent variables at their different levels on the globule size and entrapment efficiency was analysed from the generated perturbation plots, contour plots, experimental versus predicted plots, and 3D surface plots [25, 26]. Quadratic equation generated by the best-fit quadratic model is depicted in

$$Y = b0 + b1A + b2B + b3C + b12AB + b13AC + b23BC + b11A2 + b22B2 + b33C2, \quad (1)$$

where Y represents measured responses, globule size, and entrapment efficiency whereas $b0$ is the intercept and $b1$, $b2$, $b3$, $b12$, $b13$, $b23$, $b11$, $b22$, and $b33$ are the regression coefficient for the model term of A, B, and C and combination of them [27].

2.4. Determination of Dispersed Globule Size, Polydispersity Index, Surface Charge, and Morphology. The size of the dispersed globules and the PDI in the nanoemulsions was measured following dilution (50 times) in distilled water using the Zetasizer analyzer (Nano ZSP, Malvern, Worcestershire, UK) by measuring the changes in intensity of scattered light through the sample. The analysis was performed in triplicate at room temperature. The potential at the outside of the stationary layer of the dispersed globules was measured using the same Zetasizer instrument.

The morphology of the optimized nanoemulsion was determined using by polarized microscope (Nikon Instruments Inc. Melville, NY, US) and transmission electron microscopy (TEM) (JEOL JEM 1010, Tokyo, Japan). For TEM analysis, the drops of diluted samples were placed on a carbon grid and stained after drying the sample and analysed under electron microscopy operated at 80 KV at 10000X magnification.

2.5. Determination of Entrapment Efficiency of LUL within the Formulated Nanoemulsion. The entrapment of LUL within the nanoemulsion formulation was determined following the method of Hussain and team [28]. This was done by removing the unentrapped drug from the developed nanoemulsion using the dialysis bag of 10,000 to 14,000 mol wt. cutoffs (Sigma Aldrich, MO, USA). The concentration of the drug was determined by the use of a UV-visible spectrophotometer at λmax 299 nm [6]. The following equation (equation (2)) was used to determine the entrapped quantity of LUL within the formulated nanoemulsion:

$$\text{Entrapment efficiency}\,(\%) = \frac{\text{amount of drug determined in the formulation}}{\text{total drug added in the formulation}} \times 100. \quad (2)$$

2.6. Preparation Method of LUL-Loaded NEG. The optimized nanoemulsion containing the drug was developed using eucalyptus oil (15%) and Smix (3 : 1) (45%) at a homogenization time of 15 min. The NEG of the optimized nanoemulsion was developed by incorporating into Carbopol 934 to the nanoemulsion to get final polymer concentration of 0.5% (w/w) [28]. Consistent dispersion of the polymer was prepared initially in distilled water to get the hydrogel of Carbopol 934. The dispersion was kept overnight at constant stirring using magnetic stirrer (50 rpm) following the addition of triethanolamine (2-3 drops) to facilitate the formation of crosslinking between the polymeric components. Finally, the developed formulation contains an LUL concentration of 10 mg/mL in the fabricated LUL-NEG.

2.7. Determination of Viscosity, pH, and Refractive Index of the LUL Nanoemulgel. The pH of the fabricated LUL-loaded nanoemulgel was determined using calibrated pH meter, whereas the viscosity of the formulation was determined using a rotational viscometer at room temperature ($25 \pm 2^{\circ}$C). The refractive index of the optimized nanoemulgel was determined using an Abbe refractometer.

2.8. Determination of Rheological Property of the LUL Nanoemulgel. The rotational viscometer attached to the cone and plate of the Brookfield viscometer (Model DV-E, Brookfield, Middleboro, MA, USA) was used in this present study to determine the rheological properties of the LUL-NEG. The rheogram for the determination of viscosity was determined with the increasing shear rate from 0 to 200 S^{-1}. The measured values of viscosity were (Pa.s) recorded at room temperature ($25 \pm 1^{\circ}$C) and plotted the viscosity versus shear rate curve to interpret our findings.

2.9. Determination of In Vitro Antifungal Activity Using the Well-Diffusion Method. Determination of antifungal efficacy of the LUL-NEG was compared with DMSO (5%),

blank NEG, LUL gel, and LUL solution following the method described by Kadimi and group [29]. In this well, diffusion method was used where the efficacy of the formulations was tested against *Candida albicans*. Initially, the organism was cultured in sabouraud dextrose agar media (pH 6.2). Then, the media was prepared and sterilized using an autoclave (121°C for 20 min). The media was then transferred into the sterile Petri dishes aseptically in laminar flow cabinet. Just before the addition of media, the grown culture was mixed with the normal media. The Petri dishes were incubated in inverted positions at 35°C for 48 h after an hour of loading the respective formulation into the wells prepared using a cork borer. The readings were recorded as the zone of inhibition by measuring the diameters.

2.10. Animal-Based Study

2.10.1. Animal Procurement. Procured experimental Wistar rats (180 to 220 g) from registered breeder were acclimatized to the standard laboratory conditions (25 ± 2°C and 55 ± 5% relative humidity) for 7 days with free access to food and water. The animals were kept in polypropylene cages, which were maintained 12 h dark and light cycle under the standard condition. The experimental protocols were approved by the Research Ethics committee, approval number (PH-130-41), Faculty of Pharmacy, King Abdulaziz University, Jeddah, Saudi Arabia.

2.10.2. Ex Vivo Permeability Study. *Ex vivo* skin permeation study of the LUL-NEG and LUL gel formulations through the rat skin was studied using Franz diffusion cells. A freshly excised abdominal rat skin was collected after 24 h of removal of skin from the experimental animal. The freshly excised skin was washed with normal saline and the subcutaneous fat layer beneath the skin was removed. Thereafter, the skin was arranged between the donor and acceptor compartment, facing the stratum corneum of the skin towards the donor compartment and the dermis part touching the receptor compartment [28]. A 1 mL volume of the nanoemulgel was loaded to the 3.104 cm^2 diffusion area and the setup was maintained at 34 ± 1°C to mimic the skin condition. A magnetic bead was used to maintain constant stirring of the phosphate buffer (pH 7.4) in the receptor chamber. The samples (0.5 mL) were withdrawn from the receptor chamber of the diffusion cell at predetermined time intervals with the replacement of a similar volume of fresh buffer. The samples were analysed for LUL after filtration using HPLC with the mobile phase consisting of ammonium phosphate buffer (0.1 M) and acetonitrile at 60 : 40 ratio [30]. Later, the permeation parameters (apparent coefficient of permeation (Papp) and flux (Jss)) were calculated using the following equations:

$$P_{\text{app}} = \frac{\text{slope}}{\text{tissue surface area}} \times \text{volume of the donor compartment}, \tag{3}$$

$$\text{Jss} = P_{\text{app}} \times \text{concentration of LUL in the donor compartment}. \tag{4}$$

2.10.3. Skin Irritation Studies. The irritation study of the developed LUL-NEG was determined in experimental Wistar rats [31]. The acclimatized animals were used to remove the hair from the dorsal side 24 h before the study, keeping precaution of not to damage the superficial layer of the skin. The animals were then divided into four groups, where the first group was left untreated (group I; control group) and the other three groups were treated with formalin solution (0.8%) (group II, positive control), blank NEG (group III), and LUL-NEG (group IV), respectively. The formulations were applied on the cleaned skin over an area of 1 cm^2 and a similar volume of blank NEG was applied in the drug-free treatment group. The skins of the experimental animals were observed at 24 and 48 h for any dermal reactions, that is, erythema or oedema scores. The score for severe erythema or oedema is 3, where the corresponding scores of moderate, slight, and no erythema or oedema are 2, 1, and 0, respectively.

2.10.4. Histopathological Assessment of Treated Rat Skin. A portion of rat skin was exposed to different treatments, that is, control group, formalin-treated (positive control), and LUL-NEG, to determine possible topical toxicity. The animals were sacrificed using an overdose of ketamine/xylazine and the skin samples were collected by excision. Sample preparation and sectioning were carried out using a microtome. Furthermore, the sectioned samples were stained using haematoxylin and eosin dye. The staining of the samples helped in visualization of the cross-sectioned samples under microscopy. Each slide was properly visualized and imaged using an optical Leica microscope under 400 magnification.

2.11. Statistical Analysis. All the readings were measured in triplicate and the results were presented as mean ± standard deviation. The analysis of the data was performed using one-way ANOVA followed by Tukey multiple comparison test to

compare the groups of experimental results where $P < 0.05$ was considered as statistically significant findings among the groups.

3. Results and Discussion

3.1. Preparation of LUL-Loaded Nanoemulsion. Preliminary screening on solubility study of LUL in the eucalyptus oil, Tween 20, and PEG 200 revealed 74.6 ± 2.2 mg/mL, 68.3 ± 1.7 mg/mL, and 52.2 ± 1.4 mg/mL, respectively. The solubility results suggest that the desired concentration of LUL can easily be incorporated within the nanoemulsion formulation for delivery of LUL in the treatment of fungal infection. Among the tested cosurfactants (ethanol, carbitol, transcutol, and PEG 200) for the emulsification of eucalyptus oil with the help of Tween 20, we found that PEG 200 was most suitable with the higher area of nanoemulsion within the pseudoternary diagram (data not shown). Further, regarding the determination of ratio for the Smix for further processing of nanoemulsion development, we observed that 3 : 1 provides the highest area of nanoemulsion in the pseudoternary phase diagram. Therefore, the 25% cosurfactant in the Smix helps in increasing the fluidity of the surfactant significantly, which resulted in the highest nanoemulsion area in the pseudoternary phase diagram [32]. Selecting the ratio of Smix (3 : 1), the optimization of drug-loaded nanoemulsion was performed in the next stage.

3.2. Optimization of LUL-Loaded Nanoemulsion Using Box–Behnken Statistical Design

3.2.1. Optimization for Globule Size of the Nanoemulsion. Globule size is one important measure for the nanoemulsion formulation as it provides the stability, the aesthetic appeal of the nanoemulsion together with penetration through the skin [13, 33]. Therefore, the software-based optimization process was adopted in this study to optimize the globule size to reduce the experimental burden. The compositions of seventeen formulations recommended by the software are presented in Table 1. The statistical results on the effect of the interaction of process parameters such as homogenization time and the important formulation components such as oil % and % of Smix on globule size of LUL-loaded nanoemulsions are presented in Table 2. From the representation, it could be said that the model terms A, B, C, A^2, and B^2 have a statistically significant influence (P values <0.05) on the globule size of the developed formulations.

The model F-value of 85.75 and P value of <0.05 represented the significance of the used quadratic model. The predicted R^2 (0.8585) and adjusted R^2 (0.9795) values are in reasonable agreement with a difference of less than 0.2. Additionally, the desirable value for adequate precision (signal-to-noise ratio) should be greater than 4, whereas the adequate precision value of 28.962 indicated an adequate signal in the used model. Hence, this model could be used to navigate the design space. The observed and predicted values for the globule size are also in close agreement as depicted in Table 1.

A polynomial equation on the effect of the interaction of three independent variables on globule size of the developed nanoemulsion formulations was generated in the fitted model (equation (5)), where coefficient values for the model terms A (+13.68) and B (+11.01) are positive, which indicated that the globule size will increase with increasing % of oil and Smix, respectively. On the contrary, the negative coefficient value of −8.06 for the model term C indicated that increasing homogenization time resulted in decreasing globule size of the nanoemulsion. The increasing globule size with increasing oil % is in agreement with reported data [34, 35].

$$\begin{aligned} Y1 = {} & +16.33 + 13.68 * A + 11.01 * B - 8.06 * C \\ & + 20.60 * A^2 - 3.78 * A * B + 1.73 * A * C \\ & + 31.13 * B_2 + 2.79 * B * C - 1.45 * C^2. \end{aligned} \quad (5)$$

Further, the initial decrease followed by an increase in globule size of the nanoemulsion with increasing % of oil and Smix is evident in the perturbation plot and 3D surface plot (Figures 1(a) and 1(b)). The initial increase in oil % may lead to proper solubilization of LUL, which might result in a decrease in globule size, and a further increase in oil % resulted in an increase in globule size due to insufficient surfactant to effectively coat the dispersible globule. A decrease in globule size with an initial increase in surfactant % was noted which might be due to a reduction in interfacial tension between the dispersible globules and aqueous phase and provide a successful coating over the dispersible globules [34], whereas a further increase in surfactant concentration leads to an increase in globule size which might be due to formation aggregation after a certain % of Smix concentration. Increasing stirring time (model term C) resulted in decreasing the globule size, which is reflected in equation (5) by the negative coefficient value for model term C and also in perturbation plot (Figure 1(a)) with decreasing slope associated with increasing stirring time. Our findings are in agreement with the existing reported data [36]. As mentioned previously, all three model terms have a significant effect on the globule size of the formulation (Table 2). Predicted and experimental data for the globule size are in close agreement, which can be seen in the predicted versus actual plot (Figure 1(c)) and also in Table 1.

3.2.2. Optimization for Entrapment Efficiency of the Nanoemulsion. Higher % of encapsulation efficiency is one of the major targets in formulation development. During the optimization process of encapsulation efficiency of nanoemulsion formulation, the statistical outcome (Table 2) on the interaction of three independent variables indicated that model terms A, C, AC, A^2, B^2, and C^2 are significant ($P < 0.05$).

Further, the F-value of 122.76 of the model and the P value of <0.05 indicated the significance of the used quadratic model. The predicted R^2 (0.9587) and adjusted R^2 (0.9856) values are in close agreement as the difference is less than 0.2. Additionally, an adequate precision value of 32.838

Table 1: Box–Behnken statistical design: levels of three independent variables from the experimental runs along with the predicted responses on LUL-loaded nanoemulsion.

Batch	Levels of independent variables			Actual responses		Predicted responses	
	A (% v/v)	*B* (% v/v)	*C* (% v/v)	Globule size (*Y*1) (nm)	Entrapment efficiency *Y*2 (%)	Globule size (*Y*1) (nm)	Entrapment efficiency *Y*2 (%)
F1	0	−1	1	20.62	85.23	24.13	85.3
F2	0	0	0	16.67	92.86	16.33	92.74
F3	1	1	0	87.32	93.51	88.96	93.94
F4	0	1	1	54.02	86.54	46.87	86.19
F5	0	0	0	15.77	93.46	16.33	92.74
F6	1	0	−1	53.61	95.34	55.48	94.98
F7	0	0	0	17.23	91.79	16.33	92.74
F8	0	0	0	15.89	92.44	16.33	92.74
F9	−1	0	−1	32.21	85.45	31.56	85.53
F10	1	−1	0	78.63	93.56	74.49	93.57
F11	1	0	1	42.18	94.48	42.81	94.4
F12	−1	−1	0	41.23	82.46	39.59	82.03
F13	−1	0	1	13.88	79.33	12.01	79.69
F14	−1	1	0	65.02	81.32	69.16	81.31
F15	0	−1	−1	43.57	89.22	45.84	89.57
F16	0	1	−1	65.79	88.39	62.28	88.32
F17	0	0	0	16.07	93.14	16.33	92.74

Independent variable	Levels		
	Low (–1)	Medium (0)	High (1)
A = oil (% *v/v*)	10	15	20
B = Smix (% *v/v*)	35	45	55
C = homogenization time (min)	10	15	20

Dependent variables
*Y*1 = globule size (nm)
*Y*2 = entrapment efficiency (%)

Table 2: Analysis of variance data for globule size and entrapment efficiency.

ANOVA on globule size			ANOVA on entrapment efficiency		
Source	*F*-ratio	*P* value	Source	*F*-ratio	*P* value
Model	85.75	<0.0001	*Model*	122.76	<0.0001
A	124.66	<0.0001	*A*	792.44	<0.0001
B	80.84	<0.0001	*B*	0.1710	0.6916
C	43.30	0.0003	*C*	55.76	0.0001
AB	4.75	0.0657	*AB*	0.8061	0.3991
AC	0.9918	0.3525	*AC*	18.77	0.0034
BC	2.60	0.1506	*BC*	3.11	0.1213
A^2	148.84	<0.0001	A^2	39.55	0.0004
B^2	339.93	<0.0001	B^2	114.49	<0.0001
C^2	0.7407	0.4179	C^2	56.71	0.0001

indicated an adequate signal for the used model. Hence, this model could be used to navigate the design space.

A polynomial equation on the effect of the interaction of three independent variables on entrapment efficiency of the developed nanoemulsion formulations was generated (equation (6)). The positive coefficient value for the model terms *A* (+6.04) indicated that the entrapment efficiency would increase with an increasing % of oil. On the contrary, the negative coefficient of model terms *B* (−0.0887) and *C* (−1.60) indicated that the increasing % of Smix and stirring time would lead to decreasing in entrapment efficiency of the LUL nanoemulsion. However, Smix does not have a significant effect on entrapment efficiency as indicated by *P* values in Table 2.

$$Y1 = +92.74 + 6.04 * A - 0.0887 * B - 1.60 * C - 1.86 * A^2 + 0.2725 * A * B + 1.32 * A * C - 3.17 * B^2 + 0.5350 * B * C - 2.23 * C^2. \quad (6)$$

Increasing the entrapment efficiency with increasing oil % is further confirmed in perturbation plot (Figure 2(a)) with positive slope associated with increasing oil %, in contour plot (Figure 2(b)) with colour changes from blue to red with increasing oil %. A similar effect of oil on entrapment efficiency is evident in the 3D surface plot (Figure 2(c)). A higher % oil supports solubilization of the entrapped drug, which might help in enhancing the entrapment efficiency of the LUL in the formulation, whereas increasing stirring time resulted in decreasing entrapment efficiency, which could be represented by the negative slope associated with model term C (Figure 2(a)), and the finding

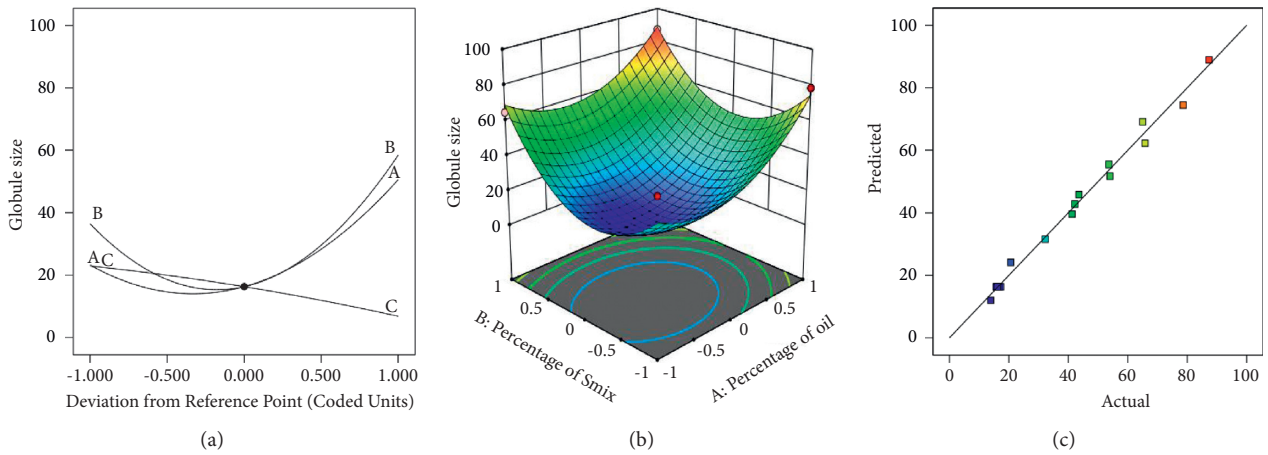

Figure 1: Consequence of independent variables on globule size. Results were presented in the (a) perturbation plot, (b) 3D surface plot, and (c) predicted versus actual graph.

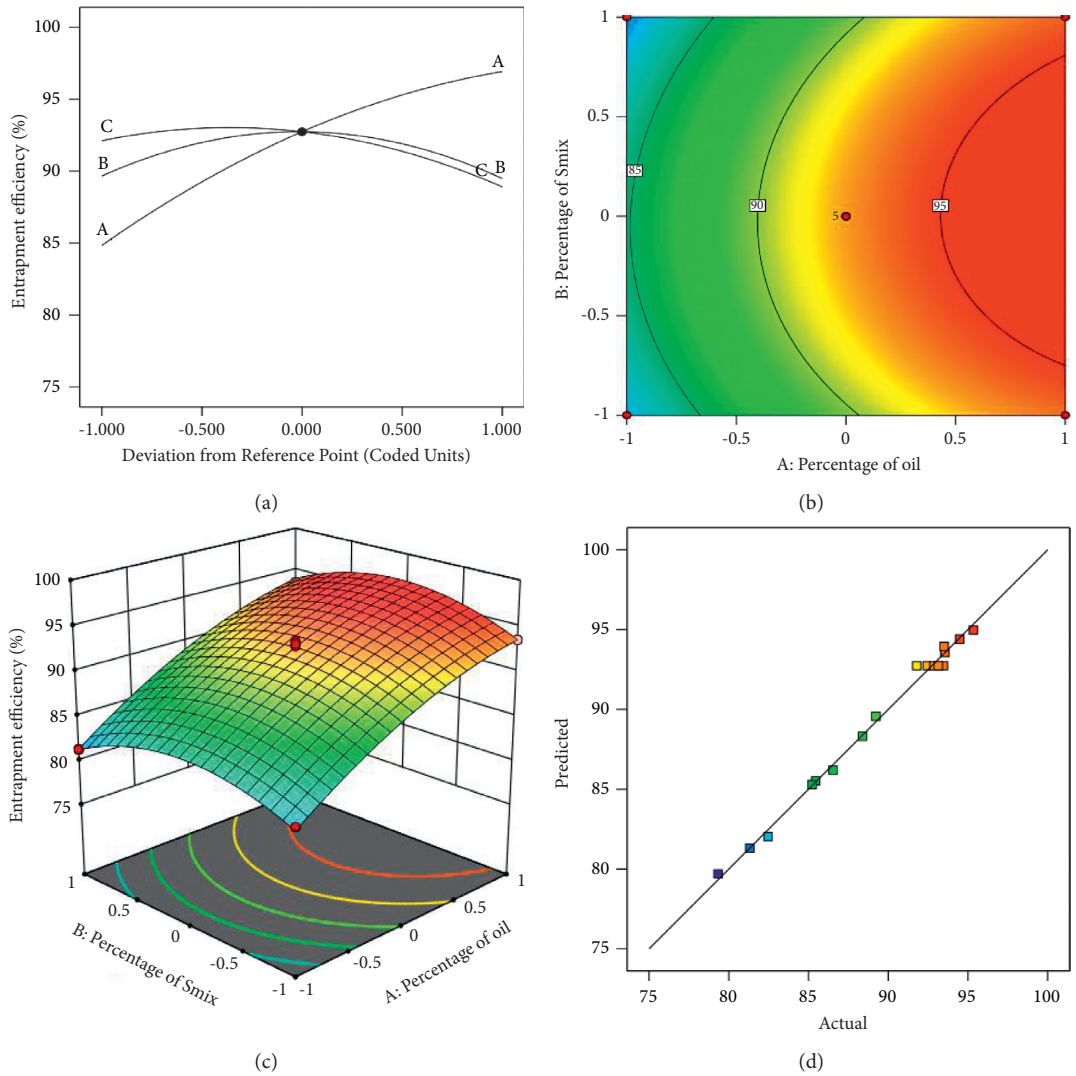

Figure 2: Consequence of independent variables on entrapment efficiency. Results were presented in the (a) perturbation plot, (b) contour plot, (c) 3D surface plot, and (d) predicted versus actual graph.

is at per the negative coefficient of stirring time in equation (6). A similar effect of stirring time on entrapment efficiency is reported in the literature [36]. The effect of % oil and stirring time on entrapment efficiency was further confirmed in the 3D surface plot (Figure 2(c)). The closeness of experimental and predicted values for the entrapment efficiency is represented in Table 1 and the predicted versus actual plot (Figure 2(d)).

3.3. Characterization of the Formulation for Globule Size, PDI, Morphology, and Zeta Potential. Being an important characterizing parameter of nanoemulsion, the size of the dispersed globules provides the stability of the formulation, whereas the nanometric lipid globule allows easy penetration from the stratum corneum. Alternatively, the PDI of the dispersion refers to the uniformity of the dispersed globule size, where the PDI <0.5 is considered as homogenous distribution [13, 32]. The results of the optimized nanoemulsion were found to be 16.67 ± 3.67 nm, where the PDI was 0.376 ± 0.022, indicating the usefulness of our drug-loaded nanoemulsion for topical application [37].

The zeta potential provides the charge on the globule surface that contributes to the stability of the formulation, where higher charges allow repulsive forces between the globules and thus prevent aggregation or coalition of the dispersed globules [38]. However, the zeta potential of the dispersed globules was found to be -9.53 ± 0.25 mV. This low zeta potential is due to the nonionic surfactant incorporated in our formulation. Incorporation of these globules in the polymeric matrix will hinder the movement of the globules, thereby imparting the stability of the formulation [15]. Further, the negative charge of the dispersed drug-loaded oil globules might be due to the presence of anionic groups in the cosurfactant and oil core [14].

Further, analysis of morphology and globule size of the developed formulation as obtained under a polarized microscope and TEM study are presented in Figures 3(a) and 3(b). The polarized microscopic and TEM micrographs represented the spherical morphology of the dispersed globules in the system. Further, the size of the globules obtained from the dynamic light scattering method is in agreement with the size found in the TEM micrograph. Our results on the morphology of the formulation are as per our previous findings [14].

3.4. Characterization of the LUL-NEG for Viscosity, pH, and Refractive Index. Carbopol is a water-soluble cross-linked polyacrylic acid polymer, widely used in topical preparation as a gelling agent. This pH-sensitive polymer has also gained popularity in pharmaceutical products as suspending, stabilizing, and emulsifying agent. The addition of triethanolamine helps to neutralize the developed formulation to form into gel at skin pH [39]. The incorporation of the formulated and optimized nanoemulsion in the prepared gel matrix of 0.5% (w/w) Carbopol 934 at a ratio of 1 : 1 produced the final NEG containing LUL.

The pH of the NEG to be applied on skin should be compatible; thus, determination of pH is important. The determination of pH of the developed LUL-NEG was found to be 5.65 ± 0.17, almost comparable to the pH of the skin. Thus, it could be said that the pH of the formulation would be favorable to the patients [14]. Further, the viscosity of the LUL-NEG was found to be 9.26 ± 0.08 Pa.s at a shear stress of 60 Pa and shear rate of $6s^{-1}$. It was found that the incorporation of optimized nanoemulsion into the blank NEG did not alter the rheological property of the formulation. Our results are in agreement with our previous findings [14], which suggest that the viscosity of the product would be in a stage to easily spread over the skin.

Further, the refractive index is an optical property where the isotropic nature of the formulation reflects no interaction between the drug and excipient. The refractive index of our optimized LUL-NEG formulation was found to be 1.31 ± 0.08, which is quite similar to water representing clear and transparent hydrogel without any interaction.

3.5. Rheological Property of the LUL-NEG. Two important parameters, adherence and spreading, are essential for the formulations to be applied topically. After equilibration of the formulation for a week, the curve was plotted to represent the relationship between shear rate and the applied stress (Figure 4). The experimental results of viscosity (Pa.s) of the LUL-NEG were found to be thixotropic characteristics with the increase in shear within the range of 20 to 200 S^{-1}. The descending lines of the presented curves (Figure 4) confirmed it. The rheological properties of the gel formulations are correlated to the preparation process, the molecular weight of the incorporated polymer, and the degree of crosslinking [40]. Based on the findings of the present investigation, it could be said that the rheological property of the formulation could be easily applied topically as the increasing rate of shear to the formulation resulted in a decrease in viscosity [41]. Therefore, to initiate a flow of the formulation, stress needs to be applied, which will facilitate easy spreadability over the topical area.

3.6. In Vitro Antifungal Efficacy. The results of the *in vitro* antifungal efficacy of DMSO (5%), blank NEG, LUL solution, LUL gel, and LUL-NEG using well-diffusion technique are presented in Figures 5(a) and 5(b). The developed and commercial NEG formulations of LUL were found to be sensitive against strain of tested fungi within the limit of our experiment. The LUL-NEG was found to inhibit the growth of *C. albicans* significantly ($P < 0.05$) when compared with other four groups (Figure 5(b)). Significant efficacy of the developed LUL-NEG formulation over LUL solution and LUL gel might be explained by the fact of incorporating eucalyptus oil in the LUL-NEG, which potentiated the efficacy of the antifungal agent. This might be due to the inherent antifungal effect of eucalyptus oil [20, 21], which was reflected by the zone of inhibition by blank nanoemulsion. Thus, the increased inhibitory effect of LUL-NEG is due to the synergistic role of LUL and eucalyptus oil when codelivered through nanoemulsion platform, which allowed intense diffusion of the drug containing oil globules. A comparable result is available in the literature where the

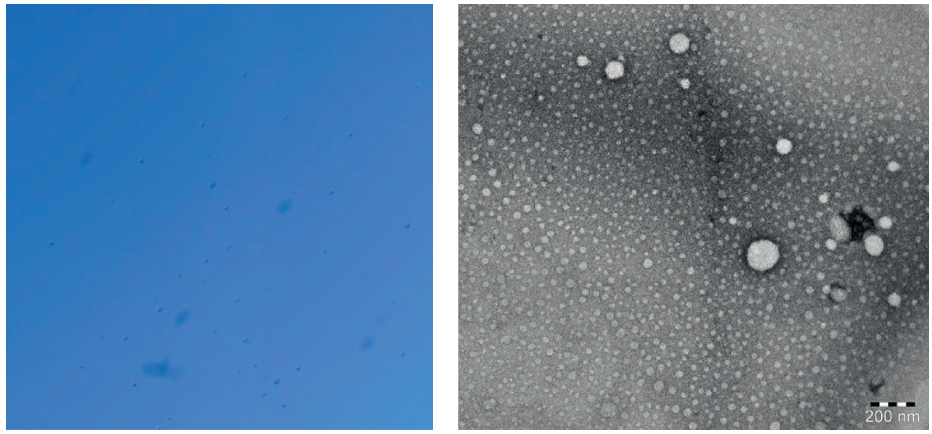

(a) (b)

Figure 3: Presentation on morphology of the optimized formulation under the polarized microscope (a) and transmission electron microscope (b).

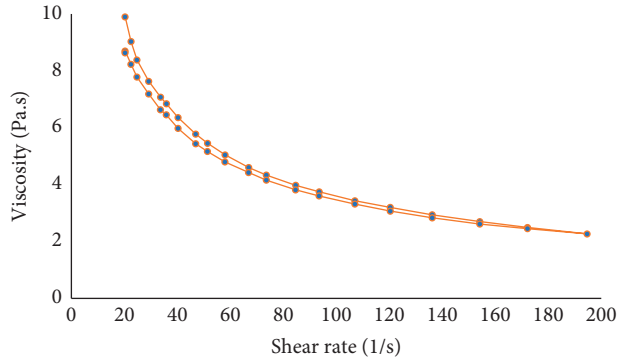

Figure 4: Viscosity versus shear rate profile of the fabricated LUL-NEG.

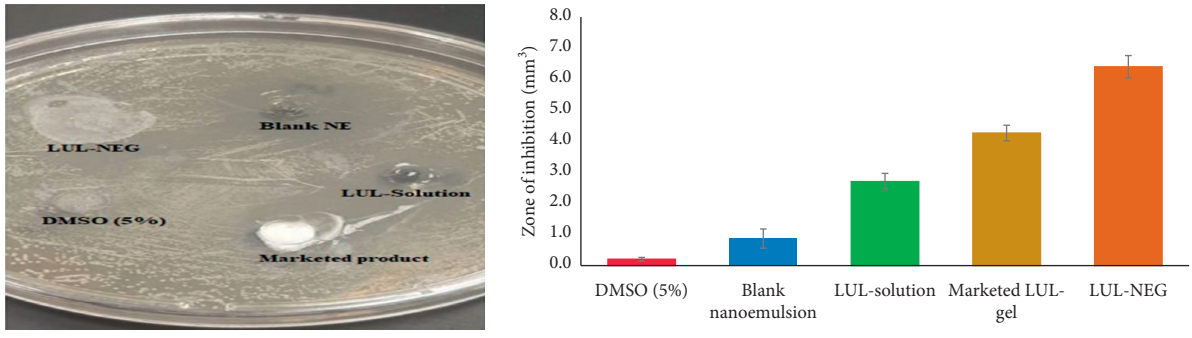

(a) (b)

Figure 5: Areas of zone of inhibition in the tested samples in the Petri dish containing *Candida albicans* (a) and the presentation of the measured area of the zone of inhibition of different groups (b). The results were presented as mean ± SD ($n = 3$). $^*P < 0.05$.

authors compared the microemulsion of LUL with the commercial formulation and reported statistically significant inhibition of growth with LUL microemulsion when compared to commercial formulation [42]. Therefore, the nanoemulsion platform containing eucalyptus oil as the oil core for LUL was found to possess superior efficacy against *C. albicans* species.

3.7. Ex Vivo Skin Permeation Study. The results of *ex vivo* permeation of LUL from the LUL-NEG and LUL gel preparation are presented in Figure 6. From the comparison on permeation profile of LUL from the two formulations, it is clearly observed that the permeation of LUL from the developed NEG formulation ($406.2 \pm 18.6\,\mu g/cm^2$) is significantly higher ($P < 0.05$) when compared to the LUL gel

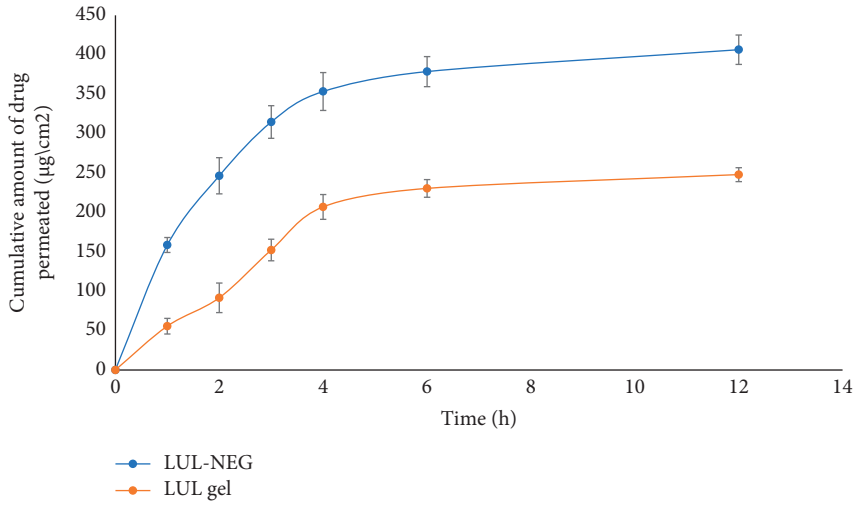

Figure 6: Cumulative amount of LUL permeation from LUL-NEG and LUL gel across the experimental rat skin. The results were presented as mean ± SD ($n = 3$).

formulation ($247.7 \pm 8.8\,\mu g/cm^2$) (Figure 6). This increased permeation might be due to the presence of nanosized oil globules containing LUL, which could increase the rate of permeation from the lipophilic layers of the skin to facilitate the permeation of the drug across the skin without any lag time [43, 44]. Simultaneously, when the permeation parameters were compared, it was found that the permeation flux was significantly enhanced ($P < 0.05$) with LUL-NEG ($37.098 \pm 1.05\,\mu g\,cm^{-2}h^{-1}$) when compared to the gel formulation ($25.37 \pm 1.21\,\mu g\,cm^{-2}h^{-1}$). A similar result was observed when the permeation coefficient of LUL-NEG ($1.289 \times 10^{-4}\,cm^{-2}h^{-1}$) and LUL gel ($0.880 \times 10^{-4}\,cm^{-2}h^{-1}$) was compared. Finally, the apparent permeation and flux of the two formulations were compared and it was found that there is an enhancement ratio of 1.46 when compared the LUL-NEG to the LUL gel formulation. This might be due to the increase of skin permeation attributable to the presence of PEG 200 [45], whereas the nanometric lipophilic globules also facilitated such permeation.

3.8. Skin Irritation Study. Compliance of the patient is of utmost importance when a novel approach of formulation is made. Any signs of irritation might restrict the use of the formulation in patients; thus, the topical preparations should be free from any irritation. Thus, to evaluate the skin irritation, the fabricated LUL-NEG was tested and compared with other groups of treated animals. The outcome of the irritation study in different groups of animals is presented in Table 3. The results of the formulations containing LUL, the fabricated and commercial, did not show any signs of irritation (erythema (redness) and edema (swelling)) even after 48 h of exposure. Alternatively, the animals in the positive control group (Group II) showed signs of irritations with a score of 2 and 3 after 24 h and 48 h of exposure, respectively [28]. Thus, it indicated that the application of formalin to the skin of the experimental animals resulted in redness and itching reaction. On the other way, the animals in groups I and III did not show any signs of erythema. Thus, from this study, it could be concluded that the polymeric blank NEG and LUL-NEG did not exhibit any signs of inflammation or irritation possessing safe delivery of the formulation to the skin for the treatment of any fungal infection.

Table 3: Erythema/oedema scores of the skin in treated animals after 24 and 48 h.

Groups	Treatment	Erythema scores	
		24 h	48 h
Control group	No treatment	0	0
Group II	(0.8% formalin solution)	2	3
Group III	Blank NEG	0	0
Group IV	LUL-NEG	0	0

3.9. Histopathological Study. To rule out any possible toxicity of the optimized formulation LUL-NEG, histopathological assessment was performed. The rat skin was treated with formalin solution as a positive control; blank NEG and LUL-NEG were compared with the control group. The examination of H&E-stained sections of control rats' skin which is formed of 3-4 layers of keratinized stratified squamous cells with normally appearing keratin layer. Furthermore, the four distinct layers of epidermis consisted of keratinized stratified squamous epithelium cells, where the layers are separated by the name, stratum corneum, stratum granulosum, stratum spinosum, and stratum basale, from outside to inside. The junction of the epidermal-dermal depicted several epidermal elevations and dermal papillae. Alternatively, the other layer, dermis, consisted of 2 layers, papillary (thin, present directly below the epidermis) and reticular layer (thick, dense irregular connective tissue). The sweat gland and sebaceous, hair follicle were seen in the dermis (Figure 7(a)). The formalin-treated group showed pathological changes such as the

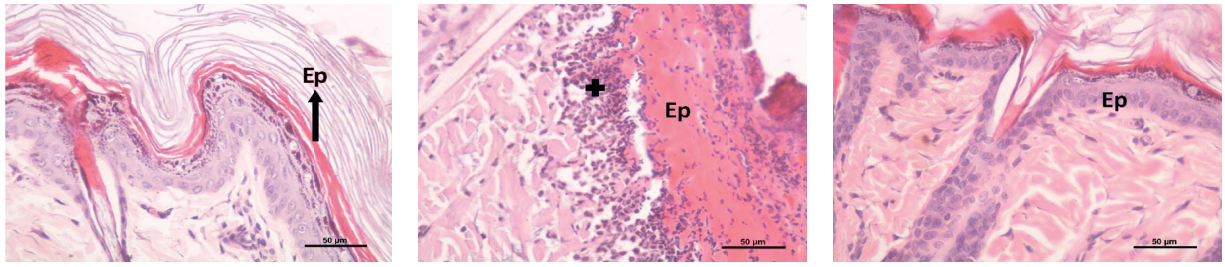

(a) (b) (c)

Figure 7: H&E staining of control skin of the rat (a) showed 3–4 layers of keratinized stratified squamous cells with normally appearing keratin layer epidermis (Ep). Formalin exposed rat skin (b) showed thickened degenerated epidermis (Ep) and inflammatory cells infiltrate (+), and LUL-NEG (c) exposed rat skin revealed no abnormal changes in the treated rat skin tissue as compared to controls (400x).

thickened degenerated epidermis (Ep), intercellular edema, and inflammatory cells infiltrate (Figure 7(b)). The LUL-NEG-treated groups (Figure 7(c)) revealed no abnormal changes in the treated rat skin tissue as compared to controls, except moderately thickened epidermis. The overall results indicated that the LUL-NEG was within the limit of the skin tolerance and safe to use for topical applications.

4. Conclusion

LUL, a broad-spectrum antifungal agent, possesses permeability and retention issues with commercially available products. Thus, the present approach of improving penetration is using the nanoemulsion platform where the mucoadhesive polymer helped to develop the NEG formulation. The development of nanoemulsion was optimized using Box–Behnken statistical design. The *ex vivo* skin permeability of LUL from the developed NEG was found to be higher when compared to the commercial formulation; thus, there was 46% improvement in flux and Papp with LUL-NEG when compared with the commercial product. Incorporation of eucalyptus oil in the preparation revealed synergistic inhibition of the tested fungi, where improved diffusion of the oil globules from the NEG facilitated the efficacy. The prepared formulation was found to be safe when applied topically on the experimental animal. There were no signs of erythema in the LUL-NEG-administered animals. Furthermore, the histopathological study demonstrated a lack of toxicity on the skin of the experimental animals, suggesting the safe and efficacious cutaneous application of the formulation. Hence, from the obtained results, it could be concluded that the LUL-NEG would be an effective approach for localized delivery of LUL safely with improved efficacy.

Data Availability

The data used to support the findings of this study are included within the article.

Conflicts of Interest

The authors declare that they have no conflicts of interest.

Acknowledgments

This study was funded by the Deanship of Scientific Research (DSR) at King Abdulaziz University, Jeddah, under grant no. RG-11–166–38. The authors, therefore, acknowledge DSR with thanks for technical and financial support.

References

[1] D. Khanna and S. Bharti, "Luliconazole for the treatment of fungal infections: an evidence-based review," *Core Evidence*, vol. 9, pp. 113–124, Sep. 2014.

[2] S. Baghel, V. S. Nair, A. Pirani et al., "Luliconazole-loaded nanostructured lipid carriers for topical treatment of superficial Tinea infections," *Dermatologic Therapy*, vol. 33, no. 6, Article ID e13959, 2020.

[3] M. H. Gold and J. T. Olin, "Once-daily luliconazole cream 1% for the treatment of interdigital tinea pedis," *Expert Review of Anti-infective Therapy*, vol. 13, no. 12, pp. 1433–1440, 2015.

[4] H. Koga, Y. Nanjoh, K. Makimura, and R. Tsuboi, "In vitroantifungal activities of luliconazole, a new topical imidazole," *Medical Mycology*, vol. 47, no. 6, pp. 640–647, 2009.

[5] H. Jerajani, C. Janaki, S. Kumar, and M. Phiske, "Comparative assessment of the efficacy and safety of sertaconazole (2%) cream versus terbinafine cream (1%) versus luliconazole (1%) cream in patients with dermatophytoses: a pilot study," *Indian Journal of Dermatology*, vol. 58, no. 1, pp. 34–38, 2013.

[6] M. Kumar, N. Shanthi, A. K. Mahato, S. Soni, and P. S. Rajnikanth, "Preparation of luliconazole nanocrystals loaded hydrogel for improvement of dissolution and antifungal activity," *Heliyon*, vol. 5, no. 5, Article ID e01688, 2019.

[7] M. Kaur, K. Singh, and S. K. Jain, "Luliconazole vesicular based gel formulations for its enhanced topical delivery," *Journal of Liposome Research*, vol. 30, no. 4, pp. 388–406, 2020.

[8] A. Mahmood, V. K. Rapalli, T. Waghule, S. Gorantla, and G. Singhvi, "Luliconazole loaded lyotropic liquid crystalline nanoparticles for topical delivery: QbD driven optimization, in-vitro characterization and dermatokinetic assessment," *Chemistry and Physics of Lipids*, vol. 234, Article ID 105028, 2021.

[9] A. K. Garg, B. Maddiboyina, M. H. S. Alqarni et al., "Solubility enhancement, formulation development and antifungal activity of luliconazole niosomal gel-based system," *Journal of Biomaterials Science, Polymer Edition*, vol. 32, no. 8, pp. 1009–1023, 2021.

[10] S. Firdaus, N. Hassan, M. A. Mirza et al., "FbD directed fabrication and investigation of luliconazole based SLN gel for

the amelioration of candidal vulvovaginitis: a 2 T (thermosensitive & transvaginal) approach," *Saudi Journal of Biological Sciences*, vol. 28, no. 1, pp. 317–326, 2021.

[11] H. Choudhury, B. Gorain, M. Pandey et al., "Recent update on nanoemulgel as topical drug delivery system," *Journal of Pharmaceutical Sciences*, vol. 106, no. 7, pp. 1736–1751, 2017.

[12] S. H. Akrawi, B. Gorain, A. B. Nair et al., "Development and optimization of naringenin-loaded chitosan-coated nanoemulsion for topical therapy in wound healing," *Pharmaceutics*, vol. 12, no. 9, p. 893, 2020.

[13] L. Y. Chin, J. Y. P. Tan, H. Choudhury, M. Pandey, S. P. Sisinthy, and B. Gorain, "Development and optimization of chitosan coated nanoemulgel of telmisartan for intranasal delivery: a comparative study," *Journal of Drug Delivery Science and Technology*, vol. 62, Article ID 102341, 2021.

[14] S. Md, N. A. Alhakamy, H. M. Aldawsari et al., "Improved analgesic and anti-inflammatory effect of diclofenac sodium by topical nanoemulgel: formulation development—in vitro and in vivo studies," *Journal of Chemistry*, vol. 2020, Article ID 4071818, 10 pages, 2020.

[15] E. Yeo, C. J. Yew Chieng, H. Choudhury, M. Pandey, and B. Gorain, "Tocotrienols-rich naringenin nanoemulgel for the management of diabetic wound: fabrication, characterization and comparative in vitro evaluations," *Current Research in Pharmacology and Drug Discovery*, vol. 2, Article ID 100019, 2021.

[16] R. L. Rajput, J. S. Narkhede, A. Mujumdar, and J. B. Naik, "Synthesis and evaluation of luliconazole loaded biodegradable nanogels prepared by pH-responsive Poly (acrylic acid) grafted Sodium Carboxymethyl Cellulose using amine based cross linker for topical targeting: in vitro and Ex vivo assessment," *Polymer-Plastics Technology and Materials*, vol. 59, no. 15, pp. 1654–1666, 2020.

[17] J. Wang, X. Wang, G. Yan, S. Fu, and R. Tang, "pH-sensitive nanogels with ortho ester linkages prepared via thiol-ene click chemistry for efficient intracellular drug release," *Journal of Colloid and Interface Science*, vol. 508, pp. 282–290, 2017.

[18] P. Sinha, S. Srivastava, N. Mishra et al., "Development, optimization, and characterization of a novel tea tree oil nanogel using response surface methodology," *Drug Development and Industrial Pharmacy*, vol. 42, no. 9, pp. 1434–1445, 2016.

[19] M. E. Elmataeeshy, M. S. Sokar, M. Bahey-El-Din, and D. S. Shaker, "Enhanced transdermal permeability of Terbinafine through novel nanoemulgel formulation; development, in vitro and in vivo characterization," *Future Journal of Pharmaceutical Sciences*, vol. 4, no. 1, pp. 18–28, 2018.

[20] H. Ramezani, H. P. Singh, D. R. Batish, and R. K. Kohli, "Antifungal activity of the volatile oil of Eucalyptus citriodora," *Fitoterapia*, vol. 73, no. 3, pp. 261-262, 2002.

[21] S. d. S. Gündel, S. N. de Godoi, R. C. V. Santos et al., "In vivo antifungal activity of nanoemulsions containing eucalyptus or lemongrass essential oils in murine model of vulvovaginal candidiasis," *Journal of Drug Delivery Science and Technology*, vol. 57, Article ID 101762, 2020.

[22] T. Adak, N. Barik, N. B. Patil et al., "Nanoemulsion of eucalyptus oil: an alternative to synthetic pesticides against two major storage insects (Sitophilus oryzae (L.) and *Tribolium castaneum* (Herbst)) of rice," *Industrial Crops and Products*, vol. 143, Article ID 111849, 2020.

[23] H. Choudhury, B. Gorain, S. Karmakar et al., "Improvement of cellular uptake, in vitro antitumor activity and sustained release profile with increased bioavailability from a nanoemulsion platform," *International Journal of Pharmaceutics*, vol. 460, no. 1-2, pp. 131–143, 2014.

[24] B. Gorain, H. Choudhury, E. Biswas, A. Barik, P. Jaisankar, and T. K. Pal, "A novel approach for nanoemulsion components screening and nanoemulsion assay of olmesartan medoxomil through a developed and validated HPLC method," *RSC Advances*, vol. 3, no. 27, pp. 10887–10893, 2013.

[25] N. A. Alhakamy, A. U. Fahmy, S. M. Badr-Eldin et al., "Optimized icariin phytosomes exhibit enhanced cytotoxicity and apoptosis-inducing activities in ovarian cancer cells," *Pharmaceutics*, vol. 12, no. 4, p. 346, 2020.

[26] S. A. Kumbhar, C. R. Kokare, B. Shrivastava, B. Gorain, and H. Choudhury, "Antipsychotic potential and safety profile of TPGS-based mucoadhesive aripiprazole nanoemulsion: development and optimization for nose-to-brain delivery," *Journal of Pharmaceutical Sciences*, vol. 110, no. 4, pp. 1761–1778, 2021.

[27] D. G. Gadhave, A. A. Tagalpallewar, and C. R. Kokare, "Agranulocytosis-protective olanzapine-loaded nanostructured lipid carriers engineered for CNS delivery: optimization and hematological toxicity studies," *AAPS PharmSciTech*, vol. 20, no. 1, 2019.

[28] A. Hussain, A. Samad, S. K. Singh et al., "Nanoemulsion gel-based topical delivery of an antifungal drug:in vitroactivity andin vivoevaluation," *Drug Delivery*, vol. 23, no. 2, pp. 642–657, 2016.

[29] U. S. Kadimi, D. R. Balasubramanian, U. R. Ganni, M. Balaraman, and V. Govindarajulu, "In vitro studies on liposomal amphotericin B obtained by supercritical carbon dioxide-mediated process," *Nanomedicine: Nanotechnology, Biology and Medicine*, vol. 3, no. 4, pp. 273–280, 2007.

[30] A. Malasiya and A. Goyal, "Method development and validation of RP HPLC method for assay and related substances of luliconazole in topical dosage form," *International Journal of Pharmaceutical Chemistry and Analysis*, vol. 4, no. 2, p. 50, 2017.

[31] P. V. Pople and K. K. Singh, "Development and evaluation of topical formulation containing solid lipid nanoparticles of vitamin A," *AAPS PharmSciTech*, vol. 7, no. 4, pp. E63–E69, 2006.

[32] H. Choudhury, B. Gorain, B. Chatterjee, U. K. Mandal, P. Sengupta, and R. K. Tekade, "Pharmacokinetic and pharmacodynamic features of nanoemulsion following oral, intravenous, topical and nasal route," *Current Pharmaceutical Design*, vol. 23, no. 17, pp. 2504–2531, 2017.

[33] B. Gorain, H. Choudhury, A. Kundu et al., "Nanoemulsion strategy for olmesartan medoxomil improves oral absorption and extended antihypertensive activity in hypertensive rats," *Colloids and Surfaces B: Biointerfaces*, vol. 115, pp. 286–294, 2014.

[34] H. Choudhury, N. F. B. Zakaria, P. A. B. Tilang et al., "Formulation development and evaluation of rotigotine mucoadhesive nanoemulsion for intranasal delivery," *Journal of Drug Delivery Science and Technology*, vol. 54, p. 101301, 2019.

[35] S. Md, N. A. Alhakamy, H. M. Aldawsari et al., "Formulation design, statistical optimization, and in vitro evaluation of a naringenin nanoemulsion to enhance apoptotic activity in A549 lung cancer cells," *Pharmaceuticals*, vol. 13, no. 7, p. 152, 2020.

[36] X. Li, L. Wang, and B. Wang, "Optimization of encapsulation efficiency and average particle size of Hohenbuehelia serotina polysaccharides nanoemulsions using response surface methodology," *Food Chemistry*, vol. 229, pp. 479–486, 2017.

[37] N. H. Che Marzuki, R. A. Wahab, and M. Abdul Hamid, "An overview of nanoemulsion: concepts of development and

cosmeceutical applications," *Biotechnology & Biotechnological Equipment*, vol. 33, no. 1, pp. 779–797, 2019.

[38] M. Pandey, H. Choudhury, O. C. Yeun et al., "Perspectives of nanoemulsion strategies in the improvement of oral, parenteral and transdermal chemotherapy," *Current Pharmaceutical Biotechnology*, vol. 19, no. 4, pp. 276–292, 2018.

[39] S. Migliozzi, G. Meridiano, P. Angeli, and L. Mazzei, "Investigation of the swollen state of Carbopol molecules in non-aqueous solvents through rheological characterization," *Soft Matter*, vol. 16, no. 42, pp. 9799–9815, 2020.

[40] A. Islam, M. Riaz, and T. Yasin, "Structural and viscoelastic properties of chitosan-based hydrogel and its drug delivery application," *International Journal of Biological Macromolecules*, vol. 59, pp. 119–124, 2013.

[41] A. Simões, M. Miranda, C. Cardoso, F. Veiga, and C. Vitorino, "Rheology by design: a regulatory tutorial for analytical method validation," *Pharmaceutics*, vol. 12, no. 9, pp. 820–827, 2020.

[42] H. Kansagra and S. Mallick, "Microemulsion-based antifungal gel of luliconazole for dermatophyte infections: formulation, characterization and efficacy studies," *Journal of Pharmaceutical Investigation*, vol. 46, no. 1, pp. 21–28, 2016.

[43] D. A. Godwin, B. B. Michniak, and K. E. Creek, "Evaluation of transdermal penetration enhancers using a novel skin alternative," *Journal of Pharmaceutical Sciences*, vol. 86, no. 9, pp. 1001–1005, 1997.

[44] S.-C. Shin and J.-S. Choi, "Enhanced efficacy of triprolidine by transdermal application of the EVA matrix system in rabbits and rats," *European Journal of Pharmaceutics and Biopharmaceutics*, vol. 61, no. 1-2, pp. 14–19, 2005.

[45] Y. Zhang, M. E. Lane, and D. J. Moore, "An investigation of the influence of PEG 400 and PEG-6-caprylic/capric glycerides on dermal delivery of niacinamide," *Polymers*, vol. 12, no. 12, pp. 2907–2911, 2020.